Support for an "A-type" Pangea reconstruction from high-fidelity Late Permian and Early to Middle Triassic paleomagnetic data from Argentina

Mathew Domeier,[1] Rob Van der Voo,[1,2] Renata N. Tomezzoli,[3] Eric Tohver,[4] Bart W. H. Hendriks,[5] Trond H. Torsvik,[2,5,6,7] Haroldo Vizan,[3] and Ada Dominguez[1]

[1]   A major disparity is observed between the late Paleozoic-early Mesozoic apparent polar wander paths (APWPs) of Laurussia and Gondwana when the landmasses are re-assembled in a conventional "A-type" Pangea. This discrepancy has endured from the earliest paleomagnetic reconstructions of the supercontinent, and has prompted discussions of non-dipole paleomagnetic fields and alternative paleogeographic models. Here we report on a joint paleomagnetic-geochronologic study of Late Permian and Early to Middle Triassic volcanic and volcaniclastic rocks from Argentina, which demonstrates support for an A-type model, without requiring modification to the geocentric axial dipole hypothesis. New SHRIMP U-Pb and ^{40}Ar-^{39}Ar isotopic dating has reinforced the inferred age of the sequences, which we estimate at ~264 Ma (Upper Choiyoi Group) and ~245 Ma (Puesto Viejo Group). Field-stability tests demonstrate that the volcanic rocks are carrying early/primary magnetizations, which yield paleopoles: 73.7°S, 315.6°E, A_{95}: 4.1°, N: 40 (Upper Choiyoi) and 76.7°S, 312.4°E, A_{95}: 7.3°, N: 14 (Puesto Viejo). A comprehensive magnetic fabric analysis is used to evaluate structural restorations and to correct for magnetization anisotropy. The paleomagnetic results derived from volcaniclastic rocks are interpreted to be affected by inclination shallowing, and corrections are discussed. A comparison of these new results with the existing Permian-Triassic paleomagnetic data from Gondwana suggests the presence of widespread bias in the latter. We contend that such bias can explain the observed APWP disparity, at least for Late Permian-Middle Triassic time, and that alternative paleogeographic reconstructions or non-dipole paleomagnetic fields do not need to be invoked to resolve the discrepancy.

Citation: Domeier, M., R. Van der Voo, R. N. Tomezzoli, E. Tohver, B. W. H. Hendriks, T. H. Torsvik, H. Vizan, and A. Dominguez (2011), Support for an "A-type" Pangea reconstruction from high-fidelity Late Permian and Early to Middle Triassic paleomagnetic data from Argentina, *J. Geophys. Res.*, *116*, B12114, doi:10.1029/2011JB008495.

1.   Introduction

[2]   It has long been recognized that the apparent polar wander paths (APWPs) of Laurussia and Gondwana are not coincident during the late Paleozoic-early Mesozoic, if a conventional reconstruction of Pangea ("Pangea A") is assumed [*Irving*, 1977; *Torsvik et al.*, 2008]. This paleomagnetic

[1]Department of Earth and Environmental Sciences, University of Michigan, Ann Arbor, Michigan, USA.
[2]Center for Advanced Study, Norwegian Academy of Science and Letters, Oslo, Norway.
[3]Departamento de Ciencias Geologicas, Universidad de Buenos Aires, Buenos Aires, Argentina.
[4]School of Earth and Geographical Sciences, University of Western Australia, Crawley, Western Australia, Australia.
[5]Geological Survey of Norway, Trondheim, Norway.
[6]Department of Physics, University of Oslo, Oslo, Norway.
[7]School of Geosciences, University of the Witwatersrand, Johannesburg, South Africa.

discrepancy has previously been attributed to a fundamental problem with the conventional paleogeographic model [*Irving*, 1977; *Morel and Irving*, 1981; *Smith and Livermore*, 1991; *Torcq et al.*, 1997; *Muttoni et al.*, 2003; *Irving*, 2004; *Muttoni et al.*, 2009] or to atypical behavior of the paleomagnetic field [*Briden et al.*, 1971; *Van der Voo and Torsvik*, 2001; *Torsvik and Van der Voo*, 2002]. Although these explanations are theoretically viable, they require an unsettling break with widely adopted models: Pangea A and the uniformitarian geocentric axial dipole hypothesis, respectively. It is therefore prudent to consider the possibility that the APWP disparity is simply an artifact of magnetic recording biases in low-fidelity paleomagnetic data [*Rochette and Vandamme*, 2001]. Supportingly, a data-filtering exercise conducted on paleomagnetic data from Baltica has demonstrated that the use of only high-quality results improves the agreement between the Permian-Triassic APWPs of Baltica and Gondwana in a conventional reconstruction [*Van der Voo and Torsvik*, 2004]. Similarly, *Domeier et al.* [2011a] have shown that Permian-Triassic paleomagnetic data from

Laurentia may be widely biased by too-shallow inclinations, and demonstrated that a correction for this bias improves the agreement between the APWPs of Laurentia and Gondwana. The remaining difference between the APWPs in both of these studies can be plausibly attributed to the lingering presence of low-fidelity data in the paleomagnetic record of Gondwana.

[3] Indeed, a review of the Permian-Triassic data from the global paleomagnetic database reveals a dearth of high-quality results from Gondwana. The majority of the paleo-magnetic results have been derived from sedimentary rocks, which are prone to a shallow inclination bias [*Tauxe et al.*, 2008], and generally associated with poor age-constraints. Many other results fail to meet modern reliability criteria, lacking either a sufficient number of samples or sites, field-stability tests, or adequate demagnetization. *Domeier et al.* [2011b] explicitly discussed the quality of Permian-Triassic paleomagnetic data from South America, and showed that by removing the data of lowest quality, the South American APWP moved closer to the APWP of Laurussia. Unfortu-nately, the filtering exercise left few results, so the APWP was defined only by three mean paleopoles with large uncertainties. Moreover, the limited number of high-quality igneous-based paleomagnetic results precluded a compara-tive test for a shallow inclination bias in the sedimentary-based paleomagnetic data.

[4] To improve the quality of the Permian-Triassic paleo-magnetic data set of Gondwana, and to further test the hypothesis that its incongruity with the corresponding Laur-ussian data (within a conventional Pangea reconstruction) could be an artifact of low-fidelity data, we present new, high-quality paleomagnetic results from Late Permian and Early to Middle Triassic rocks from Argentina. Our study has largely focused on volcanic rocks to avoid the complications of inclination shallowing in sedimentary rocks, although we present a sub-set of results that illustrate the effects of this bias. Our targeting of volcanic rocks also permits direct-dating of the sampled units, and we present results from a joint SHRIMP U-Pb and ^{40}Ar-^{39}Ar radiogenic isotope dating effort that accompanies our paleomagnetic study. A magnetic fabric analysis has been conducted on the paleomagnetic sampling sites to determine the nature of local structures and to evaluate the influence of magnetic anisotropy on the remanent magnetizations.

2. Geologic Background and Previous Paleomagnetic Studies

[5] In western and central Argentina, exposures of late Paleozoic-early Mesozoic volcano-plutonic rocks form part of a large curvilinear belt of magmatism and deformation that loosely traces the paleo-margin of southern South America (Figure 1a). Although the origin of this belt is not yet entirely clear, most studies have identified it as an inboard arc mag-matic front [*Kleiman*, 2002; *Kleiman and Japas*, 2005, 2009]. In the province of Mendoza, the late Paleozoic volcano-plutonic rocks are assigned to the Choiyoi Group, which is divided into lower (Early Permian) and upper (mid to Late Permian) subgroups (Figure 2). In the San Rafael Block (SRB) of southern Mendoza, the Choiyoi Group lies unconformably on Late Carboniferous-Early Permian

glaciomarine and fluvial sedimentary rocks of the El Imperial Formation. The Lower Choiyoi Group (called the Cochicó Group in the SRB) is a sequence of andesitic breccias and lavas, dacitic to rhyodacitic ignimbrites, and continental sedimentary rocks. The volcanic rocks follow a calc-alkaline trend and exhibit elemental distributions suggestive of an arc-affinity and derivation from a thickened crust [*Kleiman*, 2002; *Kleiman and Japas*, 2009]. Unconformably overlying the Cochicó Group is the Upper Choiyoi Group, which is subdivided into three formations in the SRB: the Agua de los Burros Formation, the Quebrada del Pimiento Forma-tion, and the Cerro Carrizalito Formation [*Rocha-Campos et al.*, 2011]. The Agua de los Burros Fm. is a volcano-sedimentary rock sequence composed of basal conglomerates and continental sedimentary rocks that yield to tuffaceous sedimentary rocks, volcanic breccias, and dacitic to rhyolitic ignimbrites and lavas that become increasingly acidic up-section. The Quebrada del Pimiento Fm. is a minor suite of shallow intrusive andesites that intrude both the Cochicó Group and the Agua de los Burros Fm. The Cerro Carrizalito Fm. is characterized by high-silica ignimbrites and lavas, but includes subvolcanic rhyolitic porphyries. The volcanic rocks of the Agua de los Burros and Cerro Carrizalito fms. exhibit a geochemical signature that is transitional between a subduction-related calc-alkaline trend and an alkaline suite indicative of an intraplate setting, whereas the intru-sive andesites of the Quebrada del Pimiento Fm. have a geochemistry more similar to that of the Cochicó Group [*Kleiman*, 2002; *Kleiman and Japas*, 2009].

[6] In the SRB, the Upper Choiyoi Group is unconform-ably overlain by the Puesto Viejo Group, a Triassic sequence of continental sedimentary rocks intercalated with volcani-clastic rocks, tuffs, basalts, and rhyolitic ignimbrites [*Kleiman and Salvarredi*, 2001]. The geochemistry of the volcanic rocks is indicative of a tensional, intraplate regime; the mildly alkaline mafic series exhibits characteristics of an enriched source, contaminated by relict arc or crustal com-ponents [*Kleiman and Salvarredi*, 1999, 2001]. The geneti-cally distinct high-silica ignimbrites of the Puesto Viejo Group appear to be extensively fractionated melts derived from a youthful crust, likely heated by a basaltic underplate from which the mafic series was derived. The sedimentary rocks of the Puesto Viejo Group are syn-rift alluvial and fluvial sandstones, siltstones, and claystones, floored by a thick clastic conglomerate containing fragments of the underlying Permian volcanic rocks. The volcaniclastic rocks, interbedded with tuffs, also contain fragments of volcanic rocks that were likely derived from the Permian substrate, as well as from re-worked pyroclastic material from contem-poraneous volcanism. *González Díaz* [1972] originally defined the Puesto Viejo Group as a formation, and divided it into lower and upper members on the basis of a coloration change in the sedimentary sequence that was attributed to a changing sediment source and/or depositional environment. *Stipanicic et al.* [2007] interpreted this poorly defined boundary as a paraconformity and elevated the Puesto Viejo formation to the rank of group; the lower and upper members were redefined as the Quebrada de los Fósiles Formation and the Río Seco de la Quebrada Formation, respectively. The Quebrada de los Fósiles Formation has been assigned an Early to Middle Triassic age according to the
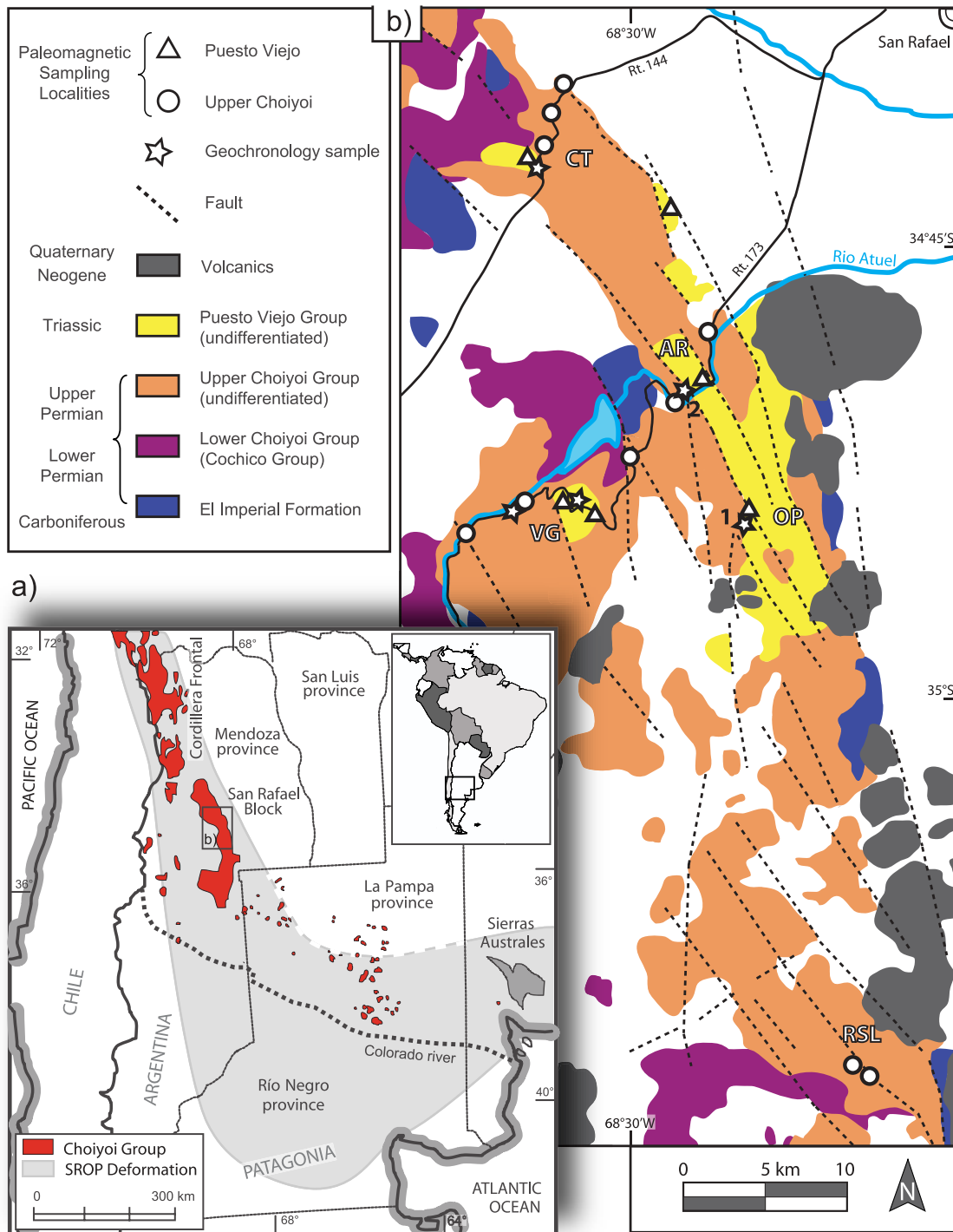
Figure 1. (a) Regional map showing the distribution of Choiyoi Group magmatism and San Rafael Orogenic Phase (SROP) deformation in central Argentina. (b) Simplified geologic map of the central San Rafael Block showing the discussed petrologic units and major paleomagnetic and geochronologic sampling localities. CT = Cuesta de los Terneros, AR = Atuel River area, VG = Valle Grande area, OP = Old Puesto area, RSL = Rio Seco los Leones; 1, 2 = location of Upper Choiyoi Group geochronology samples "PV01d" and CCH, respectively. Simplified from *Kleiman and Japas* [2009].

identification of kannemeyeriid dicynodonts [*Bonaparte*, 1982; *De Fauw*, 1993; *Domnanovich and Marsicano*, 2009], an archosauriform (*Koilamasuchus gonzalezdiazi*) [*Ezcurra et al.*, 2010], lycophytes of the genus *Pleuromeia*

[*Bonaparte*, 1982; *Artabe et al.*, 2007], and palynoflora [*Ottone and Garcia*, 1991; *Zavattieri and Batten*, 1996]. The overlying Río Seco de la Quebrada Formation is generally regarded as Middle Triassic in age, according to the
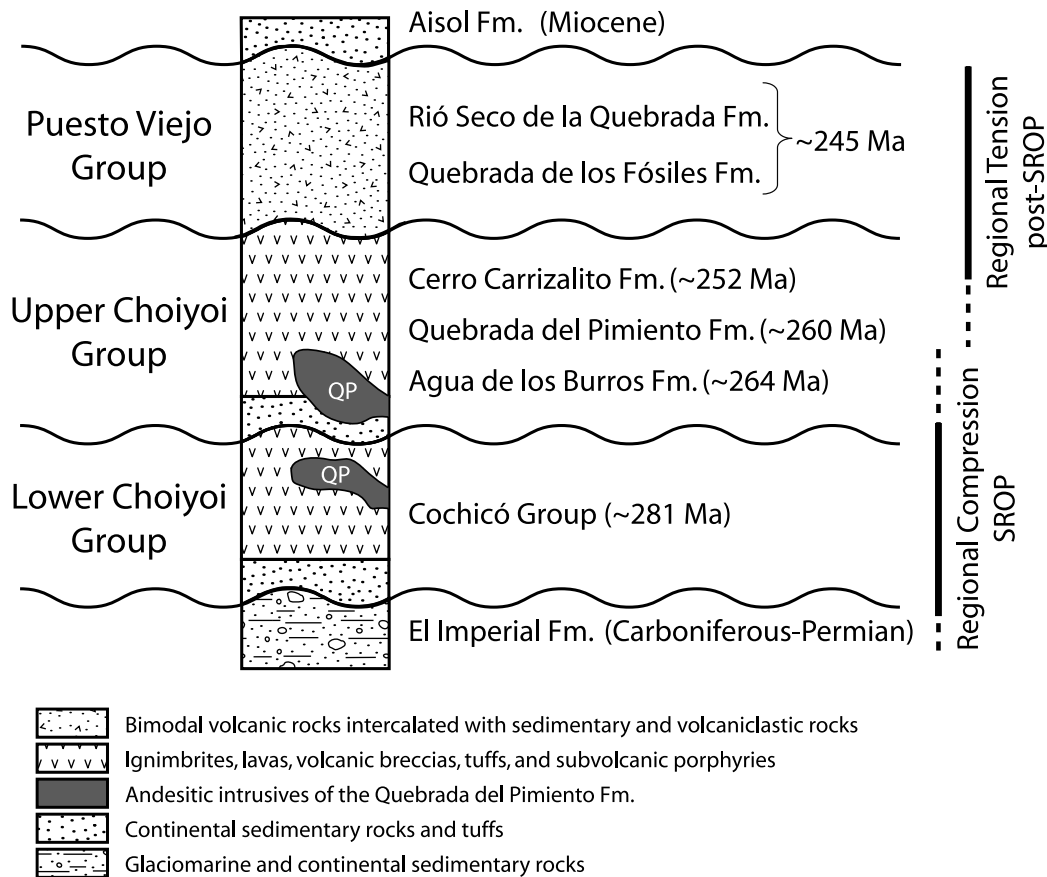
Figure 2. Schematic stratigraphy of the central San Rafael Block.

identification of cynodonts [*Bonaparte*, 1982; *Martinelli*, 2010], including *Diademodon tetragonus* [*Martinelli et al.*, 2009], and kannemeyeriid dicynodonts [*Bonaparte*, 1982; *Lucas*, 1998].

[7] Younger Mesozoic and Paleogene rocks are not known in the SRB; the Puesto Viejo Group is unconformably overlain by a mid-Miocene sedimentary rock sequence, the Aisol Formation [*Sepúlveda et al.*, 2007].

[8] In addition to the age-progressive compositional and geochemical changes observed in the late Paleozoic-early Mesozoic volcanic rocks, a co-evolving change in the regional paleo-stress (Figure 2) can be discerned from their variable deformation. In Mendoza, late Paleozoic regional shortening is assigned to the San Rafael Orogenic Phase (SROP), and is typified by NNW to NW striking faults and folds, NNE-directed thrusting, and NNE to NE trending fractures [*Kleiman and Japas*, 2009]. The earliest indication of SROP activity in the SRB may be the paleocurrent reversal observed in the late depositional stages of the El Imperial Fm. (Espejo, 1990) [*Kleiman and Japas*, 2009]. More definitive evidence of Permian shortening is found in the Cochicó Group, where growth folds and faults have been recognized, indicating that volcanism and deformation were at least partly coeval [*Cortés and Kleiman*, 1999]. Weaker deformation of the Agua de los Burros Fm. suggests that the SROP was waning during emplacement of this sequence; regional shortening is inferred to have ended prior to the emplacement

of the Cerro Carrizalito Fm. by the absence of contraction features [*Kleiman and Japas*, 2009]. Subsequent to the SROP, a post-orogenic relaxation occurred and many SROP structures were reactivated and structurally inverted through regional extension [*Japas et al.*, 2005]. Onset of this tensional phase is recognized in the Upper Choiyoi Group by injections of the Quebrada del Pimiento Fm. that exploit fracture and fault planes of post-SROP extensional structures [*Kleiman and Japas*, 2009]. NE-SW tension continued into the Triassic, evident by the syn-rift deposits of the Puesto Viejo Group, which are largely confined to narrow, NE-SW elongated fault-bound basins [*Spalletti et al.*, 1996; *Kleiman and Japas*, 2009]. Although later Mesozoic extension and Andean orogenesis occurred along the western South American margin, the SRB has remained structurally stable since the Triassic.

[9] The paleomagnetism of the Permian and Triassic sequences in the SRB were first studied by *Valencio and Mitchell* [1972], *Creer et al.* [1970, 1971], *Valencio et al.* [1975], and *Vilas and Valencio* [1982]. Notably, these early studies documented magnetizations of both normal and reverse polarity, and so provided early age constraints on the Kiaman Reversed Superchron [e.g., *Creer et al.*, 1971]. However, only blanket alternating field (AF) demagnetization treatments were routinely applied in these studies, so the resulting paleomagnetic poles must be regarded as dubious. Moreover, field stability tests were not conducted to constrain

Table 1. Summary of New ^{40}Ar-^{39}Ar Geochronology Data[a]

Sample	Type	Sep	J-Value	Steps Used	T(°C)/OP(W)	^{39}Ar(%)	Spectrum Date (Ma)	Classification	2σ	Inverse Isochron Date (Ma)	2σ	MSWD	^{40}Ar/^{36}Ar	2σ
Upper Choiyoi Group														
PV01d-2	P	K-sp	0.0058925	1 to 12	441–1276°C	99.6	255.7	Plateau	2.2	255.84	2.22917	1.8	295.0	18.2
CCH	I	WR	0.0016193	1 to 4	2.0–3.5 W	78.3	239.5	Weighted mean	7.0	240.66	13.847001	19.2	283.1	208.4
RA03d	I	Bio	0.0059674	8 to 16	786–1154°C	62.3	260.7	Plateau	2.1	258.08	4.244363	0.4	404.5	147.2
Puesto Viejo Group														
PV04d	I	K-sp	0.0017102	2 to 7	2.5–5.4 W	95.8	235.4	Plateau	2.3	235.78	3.23882	1.2	252.9	177.4
PV06d	I	WR	0.0016362	1 to 3	2.0–3.0 W	90.2	203.3	Weighted mean	13.1					
PV30d	I	WR	0.0016178	2 to 6	2.5–4.5 W	89.6	138.9	Weighted mean	4.3	144.70	3.19333	2.1	235.7	25.9
PV09d	B	Amp	0.0016305	2 to 4	3.0–4.0 W	69.9	238.6	Plateau	2.8	233.57	11.201338	0.3	357.2	127.3
PV09d	B	K-sp	0.0016263	1 to 4	2.0–3.5 W	51.2	239.3	Plateau	3.2	239.55	3.089733	0.4	259.5	77.0
PV40d	V	Bio	0.0016249	3 to 5	3.0–4.0 W	68.0	254.7	Plateau	5.0	255.10	4.997208	0.0	274.5	99.5
PV40d	V	K-sp	0.0016305	2 to 11	2.5–8.2 W	96.3	248.6	Plateau	2.3	250.59	3.695454	0.8	−260.89[b]	251.1
PV02d	I	K-sp	0.0058998	7 to 13	896–1276°C	91.8	239.2	Plateau	2.0	240.54	2.774623	0.6	200.9	120.2

[a]Type (rock type): P = volcanic porphyry, I = rhyolitic/dacitic ignimbrite, B = basalt, V = volcaniclastic rock. Sep (separate used): K-sp = K feldspar, Bio = biotite, Amp = amphibole, WR = whole rock. Steps used: heating steps used in spectrum date (spectrum plots shown in Figure 5 and the auxiliary material). T/OP: temperature (extraction by oven)/operating power (extraction by CO_2 laser). 2σ errors on the spectrum date and inverse isochron date include uncertainties in the J-value, uncertainties in the age of the flux monitors, and uncertainties in the decay constants.

[b]The ^{40}Ar/^{36}Ar value is meaningless due to very tight clustering.

the age of the magnetizations, so the possibility of remagnetization cannot be excluded. More recently, *Tomezzoli et al.* [2005] have reported paleomagnetic results from the Cochicó Group, and *Terrizzano et al.* [2005] have reported preliminary findings from a paleomagnetic study of the Quebrada del Pimiento Fm.

3. Sampling and Methodology

[10] Sampling of both the Puesto Viejo Group and the Upper Choiyoi Group was conducted in several areas in the SRB, mostly along routes 144 and 173, southwest of San Rafael, Mendoza (Figure 1). A supplementary set of Upper Choiyoi Group samples was collected from Rio Seco los Leones, ~70 km to the south of San Rafael. Paleomagnetic samples from the Puesto Viejo Group were taken from rhyolitic ignimbrites, basalts, interbedded volcaniclastic rocks and tuffs, and from clasts in the basal conglomerate (Table 1 and Figure 3). Paleomagnetic samples from the Upper Choiyoi Group were taken from dacitic to rhyolitic ignimbrites, volcanic breccias, and tuffs (Table 2 and Figure 3). We targeted rocks of the Agua de los Burros Fm., but acknowledge that the complexity of the local stratigraphy and the similarity of the Agua de los Burros and Cerro Carrizalito fms. prevent us from discounting the possibility that some samples of the latter may be included in our collection. Paleomagnetic samples were collected as cores with a gasoline-powered drill, or as hand-samples; both magnetic and solar compasses were used to orient the samples. A minimum of 5 paleomagnetic samples were collected per site. Multiple horizons within a thick cooling unit were occasionally sampled and assigned independent paleomagnetic site labels; where the resulting magnetization directions were found to be indistinct the data were combined (discussed below). Samples for isotopic age determinations were mostly collected alongside paleomagnetic samples and the naming scheme conveys the paired paleomagnetic site (samples "PV01d" and CCH are the exceptions, the locations of these are shown in Figures 1 and 3). The laboratory methods are described in the auxiliary material.[1]

4. Geochronology

4.1. Previous Work

[11] Previous K-Ar geochronologic results from late Paleozoic volcanic rocks of the SRB have been compiled by *Linares* [2007] and summarized by *Rocha-Campos et al.* [2011]. Averaged results suggest that the Cochicó Group was emplaced at ~268 Ma, and the Quebrada del Pimiento Fm., of similar intermediate composition, was emplaced at ~260 Ma. The high-silica porphyries of the Cerro Carrizalito Fm. were assigned an age estimate of ~253 Ma. *Melchor* [2000] also calculated a date for the Cerro Carrizalito Fm. from a collection of published K-Ar results, but determined a date of 261 ± 4 Ma.

[12] *Rocha-Campos et al.* [2011] presented SHRIMP U-Pb age estimates of 281.4 ± 2.5 Ma for the Cochicó Group, 264.8 ± 2.3 Ma for the Agua de los Burros Fm., and 251.9 ± 2.7 Ma for the Cerro Carrizalito Fm. An additional date of 264.7 ± 2.9 Ma was determined from a sample initially identified as of the Cerro Carrizalito Fm., but speculatively re-assigned to the Agua de los Burros Fm. in light of the older date determined.

[13] Five whole-rock K-Ar age estimates from ignimbrites and basalts of the Puesto Viejo Group, recalculated after the decay constants of *Renne et al.* [2010], range from 232 ± 10 to 240 ± 10 Ma, with an average of 235 ± 4 Ma [*Valencio et al.*, 1975].

4.2. New Results

[14] One Upper Choiyoi Group sample (labeled "PV01d") and two Puesto Viejo Group samples have yielded similar mid-to-Late Permian SHRIMP U-Pb zircon dates that range from 260.8 ± 3.2 Ma to 269.0 ± 3.2 Ma (Figure 4; auxiliary material).
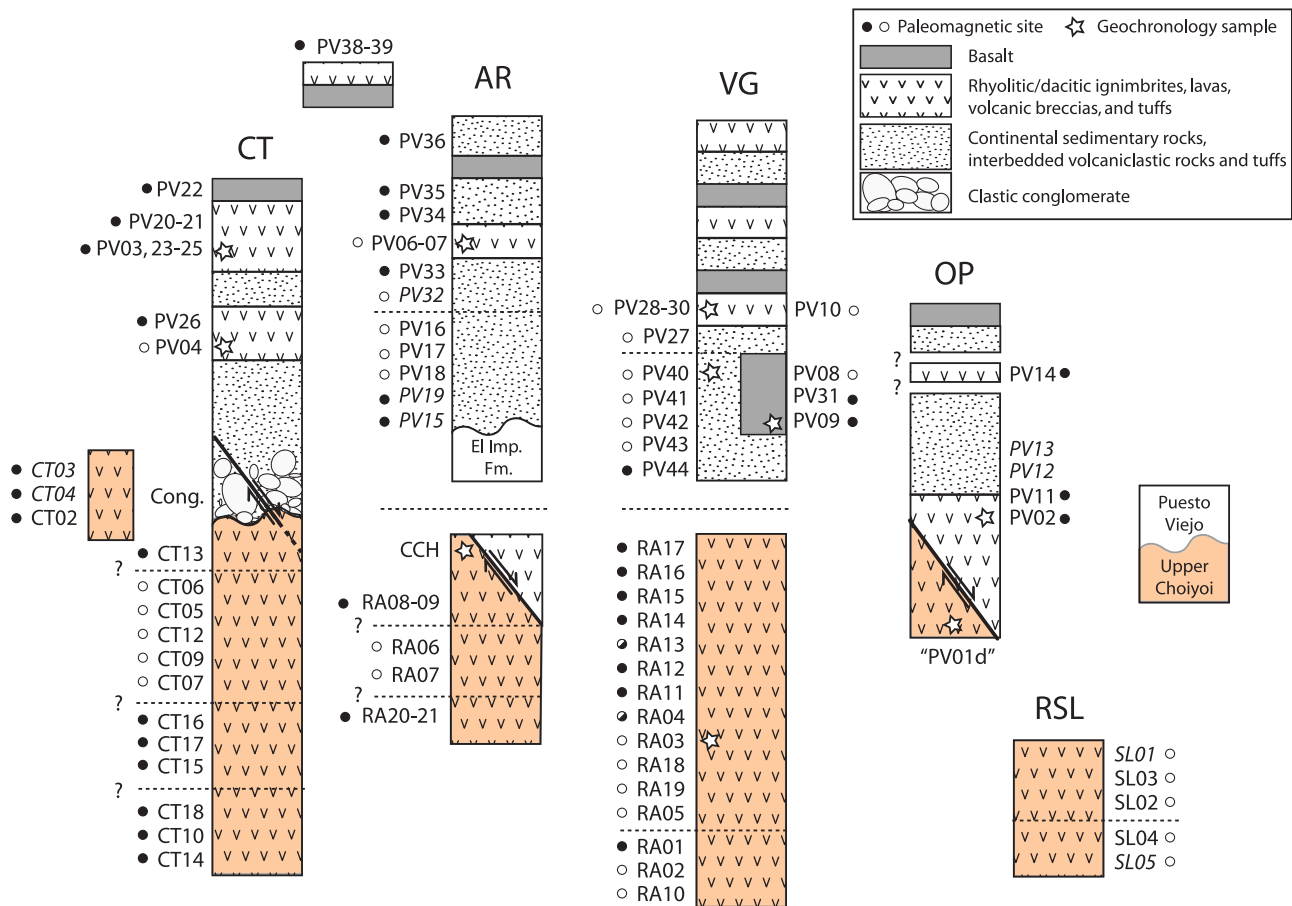

Figure 3. Simplified stratigraphy of paleomagnetic and geochronology sampling sites. CT = Cuesta de los Terneros, AR = Atuel River area, VG = Valle Grande area, OP = Old Puesto area, RSL = Rio Seco los Leones. Stratigraphic correlations have not been made between areas, so the lateral relationships between columns are not indicative of a true stratigraphic relationship (excepting the superposition of the Puesto Viejo Group on the Upper Choiyoi Group). The vertical scale is variable. Dashed lines indicate a significant break in the sequence (vertically and/or laterally). Question marks denote stratigraphic relationships that are only inferred. The filled (open) circles represent normal (reversed) polarity of the associated paleomagnetic site.

[15] ^{40}Ar-^{39}Ar dating of eleven separates from nine samples has yielded three dates from the Upper Choiyoi Group and eight from the Puesto Viejo Group (Table 3; auxiliary material). Plateau dates from volcanic rock samples of the two groups are statistically distinct (95% confidence): the Upper Choiyoi Group age estimates are Late Permian and the Puesto Viejo Group age estimates are Middle Triassic (Figure 5). Plateau dates from samples of the Puesto Viejo Group volcaniclastic rocks, however, are Late Permian and Early Triassic. Three geochronology samples exhibit discordant date spectra (step date variation exceeds analytical uncertainty) and we report weighted-mean dates for these samples. The weighted-mean dates are significantly younger than the plateau dates, ranging from Middle Triassic to Early Cretaceous (Table 3). We will return to these new results in section 9.

5. Paleomagnetic Results

5.1. Puesto Viejo Group

[16] Demagnetization of the ignimbrite samples typically results in removal of a low-temperature/coercivity component of magnetization, followed by univectorial decay to the origin (Figure 6a). This indicates that only one high-stability component of magnetization (component A) is present. The magnetization direction of the low-stability component is generally sub-parallel to the present-day dipole (PDD) or present-day field (PDF). Some sites are pervaded by a randomly oriented component of magnetization (component B) with a distributed unblocking temperature that causes the demagnetization trajectory to follow a great circle path. The great circles generally converge at a direction resembling that of the A-component (Figure 6c). AF demagnetization is found to be more effective at removing the B-component, indicating that it predominantly resides in low-coercivity grains. The random orientation of this component, its confined coercivity, and its relatively high intensity are consistent with a lightning-induced partial-remagnetization, and we do not consider it further. Laboratory unblocking temperature spectra reveal that remanence is principally lost between ~500 and 580°C. In instances where remanence persists above 600°C, the high-temperature (>580°C) fraction rarely exceeds 20% of the total remanence, and its associated

Table 2. Paleomagnetic Results From the Puesto Viejo Group[a]

Site	Type	N/n/v	Dg	Ig	Ds	Is	α_{95}	k	Strike	Dip	AMS	Slat (°S)	Slon (°W)	Plat₁	Plon₁	A₉₅₋₁	Plat₂	Plon₂	A₉₅₋₂
Cuesta de los Terneros																			
PV38	I	9/9/9	330.3	−58.2	325.2	−43.7	1.7	926.4	42	15	P	34° 43.689′	68° 28.723′	58.7	209.0	2.1	66.0	182.8	2.5
PV39	I	10/10/10	332.4	−57.6	326.9	−43.3	2.9	285.1	42	15	P	34° 43.795′	68° 28.706′	60.0	210.9	3.6	67.6	184.4	4.3
PV22	B	7/7/7	343.2	−59.8	22.9	−60.6	3.3	338.0	185	22	S	34° 42.499′	68° 34.453′	70.8	49.2	5.0	70.8	49.2	5.0
PV20	I	9/8/2	305.2	−36.1	318.6	−53.9	3.8	252.2	185	22	S	34° 42.505′	68° 34.447′	56.2	189.8	5.3	56.2	189.8	5.3
PV21	I	10/10/10	304.9	−37.1	318.8	−54.9	1.9	631.1	185	22	S	34° 42.540′	68° 34.400′	56.5	188.1	2.7	56.5	188.1	2.7
PV24	I	12/11/3	315.2	−44.3	337.0	−58.5	3.3	223.1	185	22	S	34° 42.467′	68° 34.298′	71.1	180.9	4.9	71.1	180.9	4.9
PV23	I	7/7/7	313.7	−43.3	334.3	−58.1	3.8	254.8	185	22	S	34° 42.484′	68° 34.265′	69.1	182.7	5.6	69.1	182.7	5.6
PV25	I	5/5/2	311.7	−43.2	331.8	−58.6	2.7	1081.5	185	22	S	34° 42.541′	68° 34.220′	67.1	181.5	4.0	67.1	181.5	4.0
PV03	I	17/12/6	314.4	−42.9	334.9	−57.5	3.9	234.4	185	22	S	34° 42.541′	68° 34.220′	69.6	184.5	5.7	69.6	184.5	5.7
PV26	I	7/7/5	307.8	−61.8	356.5	−75.0	3.1	395.8	185	22	S	34° 42.395′	68° 34.158′	62.8	115.0	5.7	62.8	115.0	5.7
PV04	I	8/8/7	135.5	48.2	161.2	61.8	6.8	67.7	185	22	S	34° 42.542′	68° 34.161′	−73.2	346.2	10.5	−73.2	346.2	10.5
Cong. low-T		21/12/12	7.8	−42.1	1.0	−28.0	29.3	3.2	165	15	-	34° 42.317′	68° 33.988′		R = 8.52				
Cong. high-T		21/20/20	157.8	−69.1	186.7	−85.4	71.7	1.2	165	15	-	34° 42.317′	68° 33.988′		R = 3.98				
Atuel River area																			
PV37	*T*	*5/0/0*	-	-	-	-	-	-	210	10	S	*34° 49.693′*	*68° 27.944′*	-	-	-	-	-	-
PV36	S	8/8/6	342.0	−53.9	353.6	−60.7	3.6	251.3	210	10	S	34° 49.693′	68° 27.944′	81.5	145.8	5.5	81.5	145.8	5.5
PV35	S	7/7/7	352.6	−54.8	6.1	−59.9	4.2	208.9	210	10	S	34° 49.713′	68° 27.926′	82.3	74.4	6.3	82.3	74.4	6.3
PV34	S	7/7/7	6.6	−38.0	14.4	−41.3	3.8	253.0	210	10	S	34° 49.713′	68° 27.926′	73.3	343.8	4.6	73.3	343.8	4.6
PV07	I	7/7/7	150.9	56.5	173.6	64.8	3.9	242.5	195	15	S	34° 49.698′	68° 27.873′	−77.2	311.6	6.3	−77.2	311.6	6.3
PV06	I	12/10/10	153.0	55.5	175.1	63.4	3.5	187.2	195	15	S	34° 49.698′	68° 27.873′	−79.2	310.4	5.5	−79.2	310.4	5.5
PV33	S	6/4/4	358.4	−49.4	9.8	−53.8	10.8	110.8	210	10	S	34° 49.729′	68° 27.905′	81.9	20.9	15.1	81.9	20.9	15.1
PV32	*S*	*6/5/0*	*60.8*	*11.6*	*58.6*	*16.6*	-	-	210	10	S	*34° 49.729′*	*68° 27.905′*	-	-	-	-	-	-
PV16	S	10/10/5	178.8	62.5	178.8	62.5	7.8	40.9	224	<5	P	34° 49.534′	68° 27.433′	−80.9	297.0	12.2	−80.9	297.0	12.2
PV17	S	10/10/8	175.1	50.3	175.1	50.3	3.6	184.6	224	<5	P	34° 49.534′	68° 27.433′	−84.4	62.7	4.8	−84.4	62.7	4.8
PV18	S	9/7/7	188.0	54.1	188.0	54.1	8.0	57.7	224	<5	P	34° 49.534′	68° 27.433′	−83.4	202.1	11.2	−83.4	202.1	11.2
PV19	*T*	*10/8/8*	*322.5*	*−72.7*	*322.5*	*−72.7*	*67.8*	*1.6*	224	<5	*P*	*34° 49.534′*	*68° 27.433′*	-	-	-	-	-	-
PV15	*T*	*7/6/6*	*311.7*	*−55.4*	*311.7*	*−55.4*	*50.7*	*2.7*	224	<5	*P*	*34° 49.534′*	*68° 27.433′*	-	-	-	-	-	-
Valle Grande area																			
PV10	I	8/8/8	165.6	71.2	171.4	66.7	3.4	261.2	105	≤5	P	34° 53.486′	68° 32.285′	−74.3	312.6	5.6	−66.9	312.4	5.9
PV28	I	9/9/9	108.9	68.1	177.6	69.0	4.5	132.7	145	25	S	34° 53.662′	68° 31.854′	−72.3	296.3	7.6	−72.3	296.3	7.6
PV29	I	9/8/8	163.7	70.4	176.3	68.7	7.6	53.6	150	≤5	P	34° 53.629′	68° 31.751′	−72.6	299.1	12.9	−67.3	316.4	13.1
PV30	I	10/8/8	165.3	68.5	164.4	63.5	4.5	155.9	70	≤5	P	34° 53.629′	68° 31.751′	−74.3	336.2	7.1	−70.1	318.9	7.6
PV27	S	10/10/10	163.3	56.5	171.7	54.7	5.7	64.3	150	6	S	34° 53.552′	68° 31.693′	−83.2	16.2	8.1	−76.3	7.4	8.2
PV08	B	7/7/1	186.9	67.7	178.6	64.3	5.3	172.3	45	≤5	P	34° 53.269′	68° 32.930′	−78.7	296.4	8.5	−73.5	275.9	8.9
PV31	B	9/9/9	31.8	−62.7	348.9	−66.6	5.3	96.6	0	20	P	34° 53.184′	68° 33.073′	73.6	137.9	8.7	73.6	137.9	8.7
PV09	B	10/10/10	348.4	−67.9	342.7	−63.6	5.9	68.0	45	≤5	P	34° 53.113′	68° 33.044′	73.3	158.2	9.3	71.9	135.5	9.9
PV40	S	9/9/9	173.8	62.3	178.0	55.8	2.7	354.1	107	7	P	34° 53.326′	68° 31.911′	−87.8	339.1	3.9	−80.1	318.4	4.2
PV41	S	7/7/7	178.2	57.6	181.1	50.9	3.0	417.4	107	7	P	34° 53.301′	68° 31.897′	−86.6	127.4	4.1	−86.4	314.3	4.4
PV42	S	8/7/7	176.0	56.7	179.1	50.1	2.9	438.8	107	7	P	34° 53.326′	68° 31.911′	−85.9	100.6	3.9	−86.0	343.9	4.2
PV43	S	7/7/7	170.3	58.0	174.4	51.6	4.4	193.3	107	7	P	34° 53.326′	68° 31.911′	−84.6	49.4	6.0	−81.4	352.7	6.5
PV44	S	7/5/5	343.0	−54.4	347.6	−48.4	8.1	90.9	107	7	P	34° 53.240′	68° 31.892′	78.2	225.7	10.6	76.1	196.4	11.4
Old Puesto area																			
PV14	I	10/9/9	11.9	−58.2	11.9	−58.2	4.7	119.1	0	0	S	34° 53.735′	68° 25.604′	79.7	47.8	6.9	79.7	47.8	6.9
PV13	*T*	*5/0/0*	-	-	-	-	-	-	310	40	*S*	*34° 53.832′*	*68° 25.708′*	-	-	-	-	-	-
PV12	*T*	*5/0/0*	-	-	-	-	-	-	310	40	*S*	*34° 53.860′*	*68° 25.723′*	-	-	-	-	-	-
PV11	I	11/9/6	24.5	−14.7	14.9	−52.5	8.7	53.3	310	40	S	34° 53.857′	68° 25.741′	77.5	17.5	12.0	77.5	17.5	12.0
PV02	I	13/11/10	19.9	−29.9	355.5	−64.8	7.6	52.6	310	40	S	34° 53.870′	68° 25.761′	77.7	126.2	12.2	77.7	126.2	12.2
Merged sites																			
PV38–39		19/19/19	331.4	−57.9	326.1	−43.5	1.6	434.9	42	15	P			59.4	210.0	2.0	66.8	183.6	2.4
PV20–21		19/18/12	305.1	−36.7	318.8	−54.5	1.6	458.7	185	22	S			56.4	188.8	2.3	56.4	188.8	2.3
PV03, 23–25		41/35/18	313.8	−43.7	334.8	−58.4	1.5	309	185	22	S			69.4	181.7	2.2	69.4	181.7	2.2
PV06–07		19/17/17	150.9	56.5	173.6	64.8	3.9	242.5	195	15	S			−77.2	311.6	6.3	−77.2	311.6	6.3

Merged After Tilt Corr.	N/n/v	Ds₁	Is₁	α_{95-1}	k₁	Ds₂	Is₂	α_{95-2}	k₂				Plat₁	Plon₁	A₉₅₋₁	Plat₂	Plon₂	A₉₅₋₂
PV10, 28–29	26/25/25	175.1	69.9	3.0	93.9	-	-	-	-				−70.8	300.3	5.2	-	-	-
PV10, 29–30	27/24/24	-	-	-	-	164.2	70.0	2.9	110				-	-	-	−68.0	316.7	5.0
PV09, 31	19/19/19	345.4	−65.0	3.8	79.5	349.3	−66.9	3.8	84				73.7	149.2	6.1	73.4	136.4	6.3

Anisotropy Corrected	Type	Di	Ii	Dc	Ic	α_{95}							Plat₁	Plon₁	A₉₅₋₁	Plat₂	Plon₂	A₉₅₋₂
PV38–39	ATRM	331.4	−57.9	333.2	−61.5	1.6							60.8	205.4	2.1	67.8	172.7	2.5
PV20–21	ATRM	318.8	−54.5	319.9	−56.6	1.6							57.7	185.2	2.3	57.7	185.2	2.3
PV03,23–25	ATRM	334.8	−58.4	335.3	−60.2	1.5							69.6	175.8	2.3	69.6	175.8	2.3
PV40	ATRM	173.8	62.3	174.5	67.6	2.7							−73.9	304.2	4.5	−82.8	294.5	4.1
PV41	ATRM	178.2	57.6	179.2	63.1	3.0							−80.3	294.8	4.7	−87.1	247.1	4.3
PV42	ATRM	176.0	56.7	176.7	62.3	2.9							−80.9	306.8	4.5	−88.7	277.9	4.1
PV43	ATRM	170.3	58.0	170.4	63.5	4.4							−77.5	324.3	7.0	−85.4	342.8	6.4
PV44	ATRM	343.0	−54.4	342.3	−59.9	8.1							74.9	173.3	12.2	80.1	200.4	11.3

Final Results	N	Ds₁	Is₁	α_{95-1}	k₁	Ds₂	Is₂	α_{95-2}	k₂				Plat₁	Plon₁	A₉₅₋₁	Plat₂	Plon₂	A₉₅₋₂
Volcanic rocks	14	350.8	−63.0	5.6	51.8	353.1	−64.7	5.0	63.8				−77.8	322.4	7.8	**−76.7**	**312.4**	**7.3**
Volcaniclastic rocks	13	360.0	−53.6	3.8	118.4	358.2	−56.4	4.1	103.3				−89.7	95.2	4.4	−87.0	325.0	4.9
(f = 0.8 corrected)	13	0.0	−59.4	3.5	144.2	358.3	−61.9	3.7	129.9				−84.3	292.2	4.3	−81.2	301.0	4.8
(f = 0.71 corrected)	13	0.1	−62.3	3.2	168.2	358.4	−64.6	3.4	150.0				−80.9	291.8	4.2	−77.9	297.8	4.6

direction is almost invariably parallel to that of the lower-temperature fraction (i.e., decay is univectorial) (Figure 6a). Samples from sites PV28–30 are unique in possessing a high-temperature component of magnetization (component C) that is of opposite polarity and directionally distinct (i.e., not antipodal) from the A-component in the same samples (Figure 6b). This C-component is sub-parallel to the low-temperature components and the PDD. Following from its stability and directional consistency, we designate the A-component the characteristic remanent magnetization (ChRM) of the ignimbrites (Table 1). In a few instances, a group of sites that were collected from a thick sequence of ignimbrites present statistically indistinguishable (95% confidence) site-means; these groups likely represent single cooling units. To prevent a weighting bias in the directional data set, we have averaged these sites at the sample-level (Table 1).

[17] The results of basaltic sample demagnetization are similar to those of the ignimbrites, but without a component of remanence that persists above 580°C (Figure 6d). Sites PV22 and 31 exhibit univectorial decay (component A), after removal of a low-stability component of magnetization. Remanence is lost by ~560°C in these samples. The total remanence of site PV09 is likewise eliminated by ~560°C, but a discrete decay at ~350°C is likely due to the unblocking of a distinct magnetic phase. There is typically a subtle change in the magnetization direction after removal of this intermediate temperature phase, but its site-level mean direction is not statistically indistinguishable (95% confidence) from that of the more stable phase (component A). The demagnetization trajectory of site PV08 is characterized by great circles, again due to lightning-induced partial-remagnetization. As with the ignimbrites, we designate the A-component the ChRM of the basalts (Table 1).

[18] Volcaniclastic rock samples are also dominated by univectorial decay during demagnetization (Figure 6e). A change in the demagnetization trajectory is common in the initial, low-temperature steps, and is associated with a minor, randomly oriented overprint. The remanence of these samples remains highly stable during demagnetization; through the course of thermal treatment most remanence is lost in a narrow interval between ~630 and 660°C and the laboratory unblocking temperature spectra are sharp-shouldered. AF demagnetization is ineffective (Figure 6f). There is no indication of discrete decay between ~500 and 580°C, as observed in the volcanic rock samples.

[19] Demagnetization of the clast samples from the basal conglomerate commonly reveals a low-temperature component of magnetization, oriented sub-parallel to the PDD or

PDF, that yields to a randomly oriented component at higher temperatures (Figures 6g and 6h). The high temperature component decays univectorially to the origin. In some samples, unblocking of this high temperature component is confined to the intervals of ~500–580°C and/or ~630–670°C; in others the unblocking temperatures are more distributed. A test for randomness [*Watson*, 1956] confirms that the directions of this high temperature component are statistically random at the site level (R: 3.98 < R_0: 7.17 for P = 0.05, N = 20), suggesting that the clasts preserve a primary depositional remanent magnetization (DRM) (Table 1 and Figure 6h). The directions of the low-temperature component are not statistically random (R: 8.52 > R_0: 5.52 for P = 0.05, N = 12), and they probably represent a partial viscous overprint of the PDD/PDF.

[20] Of the 42 sites collected and demagnetized, 36 have been retained for further analysis (14% rejected) (Table 1). Five of the six rejected sites were hosted in unwelded tuffs. Three of these sites (PV12, 13, 37) yielded samples that readily altered during thermal demagnetization and were highly resistant to AF demagnetization. Site-level magnetization directions from the other 2 sites (PV15, 19) were highly scattered (k < 3). Site PV32 was rejected due to a low sample-count and sub-parallel great circle demagnetization trajectories. Of the samples from the retained sites, 8% have been discarded due to alteration, erratic behavior, or anomalous magnetization directions.

5.2. Upper Choiyoi Group

[21] The demagnetization behavior of volcanic rock samples of the Upper Choiyoi Group is characteristically simple (Figure 7). Results from samples of ignimbrites, tuffs, and volcanic breccias are discussed collectively due to their similarities. Typically, a weak, low-stability component of magnetization is removed during the initial demagnetization steps, revealing a high-stability component that decays univectorially to the origin. Laboratory unblocking temperature spectra show that the high-stability component usually unblocks within the intervals of ~500–580°C and/or ~630–670°C (Figure 7). We interpret these discrete unblocking temperature intervals to reflect the presence of two distinct magnetic phases. Where co-existing, the directions of magnetization associated with these phases are typically statistically indistinct (95% confidence) at the site level, if not within the individual samples (Figure 7a). In the six sites where these directions are statistically distinct, only one pair of directions differs by more than 7° (two antipodal pairs are first inverted into a common polarity for comparison) (Figure 7d). The occurrence of antipodal high-stability

---

Notes to Table 2:

[a]Type (rock type): I = rhyolitic ignimbrite, B = basalt, T = unwelded tuff, S = volcaniclastic rock. N/n/v: (N) number of specimens measured/(n) number of specimens used in site mean calculation/(v) number of directions in (n) that are defined by vectors, rather than great circles. Dg/Ig: declination/inclination in geographic coordinates. Ds/Is: declination/inclination in tilt-corrected coordinates. α_{95}: the semi-angle of the 95% cone of confidence about the site mean direction. k: *Fisher* [1953] precision parameter. Strike/Dip: Bedding orientation determined from field observations. AMS: Interpreted nature of bedding attitude (P = primary, S = secondary) from anisotropy of magnetic susceptibility data. Slat/Slon: site latitude/longitude. $Plat_1/Plon_1$: virtual geomagnetic pole latitude/longitude determined from raw tilt-corrections. $Plat_2/Plon_2$: virtual geomagnetic pole latitude/longitude determined from AMS interpreted tilt-corrections ($Plat_1/Plon_1 = Plat_2/Plon_2$ when the bedding attitude is interpreted to be secondary). A_{95}: the semi-angle of the 95% cone of confidence about the virtual geomagnetic pole. Rejected sites are italicized. Merged sites were calculated by combining data at the sample level from multiple sites that were interpreted to represent a single cooling unit. In sites merged after tilt-correction, directions are calculated for the raw tilt-corrections (Ds_1/Is_1) and AMS tilt-corrections (Ds_2/Is_2). Magnetization directions were corrected for anisotropy by applying the inverse ATRM tensor. Di/Ii: initial declination/inclination. Dc/Ic: corrected declination/inclination.
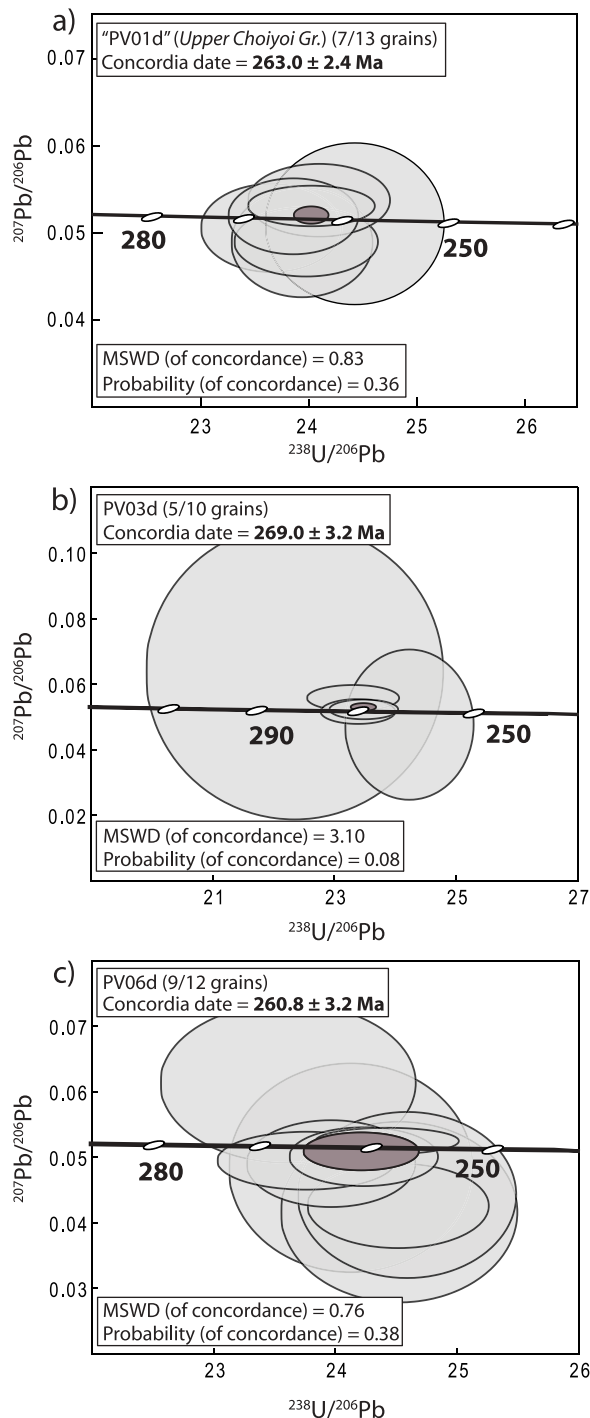
Figure 4. Tera-Wasserberg plots of SHRIMP U-Pb geochronology results. All data point error ellipses are 2σ. Darker gray ellipses depict mean results. Results from (a) an Upper Choiyoi Group volcanic porphyry, and (b, c) Puesto Viejo Group ignimbrites. See the auxiliary material for the associated data tables.

components is rare (restricted to sites RA10 and RA13; Figure 7e) and is speculatively attributed to self-reversal. The remaining sites exhibit demagnetization behavior that suggests they possess one magnetic phase exclusively (Figures 7b and 7c). In sites where the high-temperature

directions from co-existing magnetic phases have indistinguishable (95% confidence) means, we average the directions at the sample level and assign this composite direction the ChRM (Table 2). Where the mean directions of the co-existing phases are distinct, we treat both means as independent values, and weight them the same as other site means. Some pairs of sites have been collected from the same cooling unit and exhibit indistinct (95% confidence) site means; these have been averaged at the sample level to prevent a weighting bias (Table 2).

[22] Four sites (8%) have been rejected. Site CT03 is characterized by high NRM intensities and great circle demagnetization trajectories that lack a common intersection point. We assume this site has been completely overprinted by lightning. Site CT04 yields an anomalous site mean direction and is suspected to be part of a slumped block; an absence of reliable structural indicators prevent its restoration. Demagnetization of site SL01 is defined by sub-parallel great circles that prevent a determination of the ChRM direction. Site SL05 yielded highly scattered directions (k = 3.1). From the retained sites, 7% of the samples were discarded due to erratic behavior, alteration, or anomalous magnetization directions.

6. Magnetic Mineralogy

6.1. Puesto Viejo Group

[23] Thermomagnetic cycling (κ versus T) of ignimbrite samples reveals a Curie temperature at ~570°C (Figure 8a), indicative of magnetite. Hysteresis experiments show these samples to be dominated by a low-coercivity phase, corroborating the presence of magnetite, but also reveal the presence of a second, subsidiary phase with a distinctly harder coercivity (Figures 8h and 8i). The absence of a second critical point in the thermomagnetic experiments suggests that this high-coercivity phase has a low intrinsic magnetic susceptibility. These characteristics are consistent with hematite, as is the observation of a stable remanence that survives thermal demagnetization at 600°C (Figure 6a). Low temperature remanence experiments reveal a change in the rate of remanence loss during warming through the interval of ~110–120 K (Figure 8d), which is diagnostic of the Verwey transition of magnetite [*Muxworthy and McClelland*, 2000]. The natural remanent magnetization (NRM) of an undemagnetized sample is observed to decay across this transition (Figure 8e), demonstrating that magnetite carries at least part of the NRM. In some cases, the Verwey transition is suppressed and remanence is observed to decay monotonically during warming from 20 K. This behavior can reflect the presence of partially oxidized magnetite, the unblocking of superparamagnetic (SP) grains, or the re-organization of domains in multidomain (MD) magnetite [*Dormann et al.*, 1997; *Moskowitz et al.*, 1998; *Bowles et al.*, 2009]. In the low-temperature cycling of an IRM imparted at room temperature, a broad Morin transition can be observed between ~260 K and 160 K, corroborating the presence of hematite [*Özdemir et al.*, 2008]. FORC diagrams from ignimbrite samples exhibit the hallmarks of pseudo-single domain (PSD) magnetite: self-closing inner contours and outer contours which diverge toward Hc = 0 [*Roberts et al.*, 2000; *Carvallo et al.*, 2006] (Figure 8j).

[24] Thermomagnetic curves of basalt samples exhibit a Curie point at ~550°C (Figure 8b), which we interpret as the

Table 3. Paleomagnetic Results From the Upper Choiyoi Group[a]

Site	Type	Min	N/n/v	Dg	Ig	Ds	Is	α_{95}	k	Strike	Dip	AMS	Slat	Slon	Plat$_1$	Plon$_1$	A$_{95-1}$	Plat$_2$	Plon$_2$	A$_{95-2}$
Cuesta de los Terneros																				
CT03	*I*	*M*	*9/9/3*	*281.0*	*−6.1*	*283.0*	*−5.4*	*22.7*	*5.7*	*100*	*20*	*P*	*34° 40.128′*	*68° 32.701′*	*-*	*-*	*-*	*-*	*-*	*-*
CT04	*I*	*B*	*5/5/5*	*25.4*	*−30.3*	*25.4*	*−30.3*	*11.4*	*46.2*	*?*	*?*		*34° 40.178′*	*68° 32.741′*	*-*	*-*	*-*	*-*	*-*	*-*
CT02	BV	M	6/6/6	18.7	−58.2	15.8	−38.4	5.7	137.3	100	20	P	34° 40.114′	68° 32.725′	70.9	342.3	6.8	74.5	42.7	8.4
CT13[1]	I	M	6/6/6	352.0	−65.1	7.0	−52.9	3.7	325.3	126	15	P	34° 42.608′	68° 34.082′	84.1	11.4	5.1	76.2	134.8	6.0
CT13[2]	I	H	6/6/6	344.4	−69.9	5.1	−58.4	2.3	886.9	126	15	P	34° 42.608′	68° 34.082′	84.0	70.4	3.4	68.0	136.5	4.0
CT06	I	B	7/6/6	176.6	63.4	181.0	48.7	4.1	218.1	100	15	P	34° 42.333′	68° 33.987′	−84.9	120.8	5.4	−79.4	304.7	6.5
CT05	I	B	9/9/9	184.6	61.8	178.3	46.4	3.9	178.9	75	16	P	34° 42.317′	68° 33.988′	−82.9	99.2	5.0	−81.0	269.5	6.0
CT12	I	B	6/6/6	203.4	73.7	178.9	53.5	7.8	74.6	70	23	P	34° 42.317′	68° 33.988′	−88.9	57.6	10.9	−60.7	267.2	14.0
CT09	I	H	6/6/6	171.5	67.2	185.1	51.0	4.0	278.2	115	18	P	34° 42.229′	68° 33.894′	−84.7	167.7	5.4	−73.5	311.0	6.6
CT07	I	B	9/9/9	162.3	66.3	174.8	51.0	3.6	209.2	105	17	P	34° 42.223′	68° 33.849′	−84.7	55.1	4.9	−70.8	329.1	5.9
CT16	T	B	7/7/7	14.3	−59.0	357.5	−67.7	4.1	217.1	320	12	S	34° 39.590′	68° 33.000′	73.9	117.1	6.9	73.9	117.1	6.9
CT17	T	B	6/5/3	5.0	−59.1	346.0	−66.2	10.3	64.6	320	12	S	34° 39.590′	68° 33.000′	72.6	144.0	16.9	72.6	144.0	16.9
CT15	T	H	5/4/1	9.9	−64.8	345.4	−72.3	5.5	299.9	320	12	S	34° 39.590′	68° 33.000′	65.2	130.2	9.7	65.2	130.2	9.7
CT18	I	M	7/6/4	331.4	−67.3	345.6	−54.4	10.1	51.2	100	15	S	34° 41.074′	68° 33.540′	78.2	196.2	14.2	78.2	196.2	14.2
CT10	I	M	8/5/5	327.1	−73.5	346.7	−60.7	10.3	56.5	100	15	S	34° 40.651′	68° 33.117′	77.4	163.4	15.7	57.3	142.3	18.5
CT14	I	M	8/8/8	332.3	−79.8	354.5	−66.1	3.3	280.6	100	15	S	34° 40.536′	68° 33.278′	75.6	126.3	5.4	75.6	126.3	5.4
Atuel River area																				
RA08	I	B	7/6/6	355.8	−65.5	3.8	−50.3	3.8	397.3	108	16	P	34° 47.756′	68° 27.250′	85.1	333.1	5.1	76.8	124.0	6.2
RA09	I	B	7/7/7	355.6	−63.4	3.2	−48.2	4.1	217.9	108	16	P	34° 47.798′	68° 27.246′	83.8	318.3	5.4	79.3	128.5	6.5
RA06	I	H	7/7/7	226.9	81.5	147.3	76.1	4.5	181.7	23	15	S	34° 51.240′	68° 30.460′	−54.9	316.1	8.3	−54.9	316.1	8.3
RA07	I	H	7/7/7	191.8	82.4	137.8	72.0	2.6	532.7	23	15	S	34° 51.240′	68° 30.460′	−54.1	330.3	4.6	−54.1	330.3	4.6
RA20	I	B	7/7/7	22.3	−53.8	6.0	−65.6	4.8	161.8	323	15	S	34° 50.018′	68° 28.175′	76.3	94.3	7.8	76.3	94.3	7.8
RA21	I	B	7/7/7	20.7	−55.1	2.8	−66.5	2.8	466.9	323	15	S	34° 49.902′	68° 28.066′	75.7	104.1	4.6	75.7	104.1	4.6
Valle Grande area																				
RA17	I	M	7/7/7	349.7	−59.1	342.6	−47.2	3.9	234.6	52	13	P	34° 53.067′	68° 34.411′	73.8	220.3	5.1	80.4	167.0	5.8
RA16	I	H	7/7/7	19.8	−56.1	6.7	−47.9	2.3	714.1	52	13	P	34° 53.067′	68° 34.411′	81.8	337.2	3.0	73.9	33.5	3.3
RA15	I	M	7/6/6	3.6	−59.8	352.8	−49.2	6.0	127.1	52	13	P	34° 52.970′	68° 34.379′	82.3	237.8	7.9	83.6	86.3	9.0
RA14	I	M	7/7/7	3.0	−59.8	352.3	−49.2	6.6	83.7	52	13	P	34° 52.970′	68° 34.379′	81.9	235.8	8.7	83.8	90.0	10.0
RA13[1]	VB	M	7/6/6	161.9	71.7	154.0	59.2	7.9	72.6	52	13	P	34° 52.970′	68° 34.379′	−68.8	359.9	11.8	−65.1	315.5	13.9
RA13[2]	VB	H	7/7/7	353.4	−66.6	343.1	−54.9	5.1	140.2	52	13	P	34° 52.970′	68° 34.379′	76.2	194.4	7.2	75.0	128.3	8.4
RA12	I	B	7/7/7	338.6	−56.8	334.6	−44.2	4.1	213.6	52	13	P	34° 52.970′	68° 34.379′	66.4	216.8	5.1	72.6	186.9	5.9
RA11	I	B	6/6/6	329.7	−55.5	327.9	−42.6	9.3	52.5	52	13	P	34° 52.970′	68° 34.379′	60.5	212.9	11.5	65.4	189.9	13.3
RA04[1]	I	M	8/8/8	347.0	−66.0	338.9	−53.8	3.8	209.6	52	13	P	34° 52.969′	68° 34.395′	72.7	197.1	5.3	73.5	143.1	6.2
RA04[2]	I	M	8/4/4	175.9	60.7	166.8	49.3	11.6	71.6	52	13	P	34° 52.969′	68° 34.395′	−75.9	40.6	15.4	−82.5	315.4	17.7
RA03[1]	I	M	9/9/9	170.7	48.9	165.3	37.2	3.4	229.8	52	13	P	34° 52.969′	68° 34.395′	−70.9	65.2	4.0	−80.7	51.7	4.5
RA03[2]	I	H	9/8/8	172.0	54.1	165.4	42.5	2.6	200.7	52	13	P	34° 52.969′	68° 34.395′	−73.7	56.7	3.2	−83.4	21.2	3.6
RA18	I	B	7/7/7	193.5	75.3	170.1	65.1	2.6	534.3	52	13	P	34° 52.989′	68° 34.756′	−75.7	319.6	4.2	−61.3	278.4	4.8
RA19	I	B	7/7/7	165.4	57.8	159.6	45.6	4.3	101.9	52	13	P	34° 52.989′	68° 34.756′	−70.9	40.0	5.5	−77.8	0.2	6.3
RA05	I	H	7/7/7	221.5	77.5	181.5	70.5	2.8	457.3	52	13	P	34° 53.052′	68° 34.804′	−70.2	288.8	4.8	−50.5	266.4	5.1
RA01	I	H	8/6/5	1.8	−57.1	349.8	−60.6	9.4	54.0	330	8	S	34° 54.173′	68° 37.003′	79.6	158.3	14.3	79.6	158.3	14.3
RA02[1]	I	M	7/5/5	177.7	64.3	160.9	67.0	13.5	33.1	330	8	S	34° 54.435′	68° 37.088′	−69.7	329.0	22.4	−69.7	329.0	22.4
RA02[2]	I	H	7/7/7	210.4	70.4	193.6	76.8	4.5	183.0	330	8	S	34° 54.435′	68° 37.088′	−59.0	280.2	8.4	−59.0	280.2	8.4
RA10[1]	I	M	7/7/7	176.1	40.7	165.5	54.9	3.3	341.2	295	17	S	34° 54.613′	68° 37.142′	−78.1	14.9	4.7	−78.1	14.9	4.7
RA10[2]	I	H	7/5/5	170.6	46.3	155.5	59.1	12.3	39.5	295	17	S	34° 54.613′	68° 37.142′	−70.0	359.8	18.4	−70.0	359.8	18.4
Rio Seco los Leones																				
SL01	*I*	*M*	*6/6/0*	*297.3*	*16.6*	*293.7*	*−2.6*	*-*	*-*	*149*	*20*	*P*	*35° 12.142′*	*68° 19.560′*	*-*	*-*	*-*	*-*	*-*	*-*
SL03	I	H	7/7/7	136.7	63.9	173.2	58.8	2.1	473.5	141	20	P	35° 12.083′	68° 19.613′	−83.1	341.1	3.1	−55.9	350.5	3.3
SL02	I	B	6/5/5	142.0	65.1	189.6	76.2	5.9	182.0	198	19	P	35° 12.011′	68° 19.572′	−60.7	283.0	10.9	−59.4	347.0	9.5
SL04	I	B	7/7/7	152.3	69.4	193.2	67.1	2.8	806.7	165	16	P	35° 12.492′	68° 18.954′	−72.5	262.4	4.6	−63.6	330.6	4.8
SL05	*VB*	*H*	*7/7/4*	*207.6*	*36.7*	*212.7*	*24.4*	*41.0*	*3.1*	*155*	*15*	*P*	*35° 12.484′*	*68° 18.865′*	*-*	*-*	*-*	*-*	*-*	*-*
Averaged site means																				
RA08-09			14/13/13	355.6	−64.3	3.4	−49.1	2.6	281.5	108	16	P			84.4	322.8	3.4	78.3	126.7	4.2
RA20-21			14/14/14	21.5	−54.4	4.5	−66.0	2.5	253.6	323	15	S			76.1	99.1	4.1	76.1	99.1	4.1
RA14-15			14/13/13	3.3	−59.8	352.5	−49.2	4.0	108.1	52	13	P			82.1	236.7	5.3	83.7	88.1	6.0

Anisotropy Corrected			Type	Di	Ii	Dc	Ic	α_{95}							Plat$_1$	Plon$_1$	A$_{95-1}$	Plat$_2$	Plon$_2$	A$_{95-2}$
CT13			AMS	352.0	−65.1	352.0	−68.8	3.7							82.4	41.5	5.3	71.6	127.1	6.3
CT06			AMS	176.6	63.4	176.6	65.0	4.1							−86.2	126.9	5.5	−77.4	302.2	6.6
CT05			AMS	184.6	61.8	184.6	63.7	3.9							−84.3	92.7	5.1	−78.8	274.5	6.2
CT07			AMS	162.3	66.3	162.3	68.9	3.6							−86.6	31.7	5.0	−68.3	321.6	6.1
RA20-21			AMS	4.5	−66.0	4.5	−68.1	2.5							73.3	101.7	4.2	73.3	101.7	4.2
RA17			AMS	349.7	−59.1	349.7	−60.4	3.9							74.1	216.4	5.1	79.6	159.7	5.9
RA14-15			AMS	3.3	−59.8	3.3	−61.3	4.0							82.5	226.7	5.4	82.1	93.5	6.2
RA13			AMS	161.9	71.7	161.9	72.4	7.9							−68.6	357.8	11.9	−64.2	313.9	14.0
RA18			AMS	193.5	75.3	193.5	75.9	2.6							−74.9	319.4	4.2	−60.4	279.2	4.8
RA19			ATRM	165.4	57.8	168.6	64.5	4.3							−73.7	22.3	5.9	−75.7	324.9	6.9
RA10			AMS	165.5	54.9	165.5	57.3	3.3							−78.0	2.7	4.8	−78.0	2.7	4.8

Final Results	N	Ds$_1$	Is$_1$	α_{95-1}	k$_1$	Ds$_2$	Is$_2$	α_{95-2}	k$_2$						Plat$_1$	Plon$_1$	A$_{95-1}$	Plat$_2$	Plon$_2$	A$_{95-2}$
B	14	352.4	−58.2	6.3	40.2	349.0	−66.9	4.2	89.1						−82.3	334.5	7.8	−73.0	315.0	6.5
H	14	350.9	−61.4	6.5	38.8	349.5	−67.9	5.6	52.2						−78.1	326.3	8.5	−71.3	312.2	8.6
M	12	349.9	−54.8	6.5	45.8	351.0	−63.3	5.0	77.0						−81.3	8.6	7.3	−77.0	321.8	6.8
All	40	351.1	−58.3	3.6	41.4	349.8	−66.2	2.7	69.6						−81.0	340.2	4.4	**−73.7**	**315.6**	**4.1**

Curie temperature of low-Ti titanomagnetite. A sample from site PV09 reveals a critical point at ~375°C (Figure 8b), in agreement with the discrete unblocking at ~350°C observed during thermal demagnetization. The magnetic phase associated with this change is evidently metastable, as the heating curve is not reversible. Hysteresis loops and back-field curves do not show evidence of a second phase (Figures 8h and 8i), so the intermediate and high-temperature phases may share a common, low coercivity. The thermal instability and low coercivity of the intermediate temperature phase are consistent with maghemite, which could have developed by secondary, low-temperature oxidation of primary titanomagnetite. Low temperature remanence experiments on a sample from site PV09 show monotonic remanence loss above ~50 K and a suppressed Verwey transition (Figure 8f); these can be expressions of partially oxidized magnetite [*Bowles et al.*, 2009]. Low temperature cycling of an IRM imparted at room temperature reveals a broad loss of remanence during cooling that could similarly reflect the presence of maghemite. FORC diagrams exhibit indications of both PSD and MD magnetite (Figure 8k).

[25] Volcaniclastic rock samples exhibit a Néel temperature at ~660°C during thermomagnetic cycling (Figure 8c), indicating the presence of hematite. The minor change in susceptibility at ~350°C in sample PV43–2, which is not reflected in the laboratory unblocking temperature spectra, may be the expression of a minor population of magnetite or maghemite; this phase is destroyed by heating in air. Hysteresis loops and back-field curves reveal the presence of a single, high-coercivity phase, consistent with hematite (Figures 8h and 8i). Low temperature remanence experiments yield a discernable Verwey transition (Figure 8g), establishing the presence of magnetite in these rocks. The Morin transition is not evident in these experiments, perhaps because the capacity of hematite to acquire a low-temperature remanence is negligible, relative to magnetite. A broad Morin transition can instead be seen between ~260 K and 150 K in the low-temperature cycling of an IRM imparted at room temperature. The suppression of the Morin transition below ~262 K has been observed to relate to grain size, cation substitution, and the density of lattice defects, implying that the hematite in these samples is either fine grained (≤~0.1 μm) or non-stoichiometric [*Ericsson et al.*, 1986; *Özdemir et al.*, 2008; *Jacob and Abdul Khadar*, 2010]. The observation of nanoparticle-like behavior – monotonic decay of low-temperature IRMs during warming and progressive blocking of room temperature IRMs with decreasing temperature – in many of the volcaniclastic rock samples may be due to a population of SP grains [*Dormann et al.*, 1997].

6.2. Upper Choiyoi Group

[26] Thermomagnetic curves of ignimbrite samples reveal Curie temperatures of ~560–580°C and Néel temperatures of ~645–660°C (Figures 9a and 9b), which are consistent with the presence of magnetite and hematite, respectively. As deduced from the demagnetization results, some samples appear to possess both phases, whereas others reveal the presence of either phase in isolation. Hysteresis experiments corroborate the presence of at least two distinct phases: low- and high-coercivity fractions, compatible with our magnetite and hematite assignments (Figures 9g and 9h). "Goosenecked" and "wasp-waisted" hysteresis loops result from the mixing of these low- and high-coercivity components in various proportions [*Tauxe et al.*, 1996]. A widespread occurrence of magnetite in these samples is confirmed by the common observation of the Verwey transition in low-temperature remanence experiments (Figures 9c and 9e). It is evident that magnetite acts as a carrier of the NRM by the discrete low-temperature demagnetization of the NRM between ~100 K and 120 K in an undemagnetized sample (Figure 9d). The Morin transition is also apparent in many samples as a broad interval of remanence loss between ~260 K and 140 K during low-temperature cycling of a room temperature IRM (Figure 9f). FORC diagrams exhibit a range of coercive behavior, but PSD- and MD-like results are the most common (Figures 9i and 9j).

7. Magnetic Fabrics

7.1. Anisotropy of Magnetic Susceptibility

[27] Magnetic anisotropy is the orientation-dependence of any magnetic property, and the quantification of this dependence is widely used as a tool for petrofabric analysis. Results of magnetic anisotropy measurements are routinely presented as ellipsoids, which are representative of a best fitting second-rank tensor. The principal axes (K_{max}, K_{int}, K_{min}) of an ellipsoid are parallel to the eigenvectors of the matrix, and scaled according to the associated eigenvalues. Because measured magnetic properties are integrative, anisotropy will be a composite function of all the combined mineralogic sources. In felsic volcanic rocks, the anisotropy of low-field magnetic susceptibility (AMS) is typically controlled by accessory (titano-) magnetite, which has a susceptibility that is 2 to 3 orders of magnitude greater than that of hematite and most paramagnetic minerals, and ~6 orders of magnitude greater than diamagnetic materials [*Rochette et al.*, 1992]. Given the predominance of magnetite in the Puesto Viejo Group and Upper Choiyoi Group volcanic rocks, we assume this mineral controls their AMS.

Notes to Table 3:

[a]Type (rock type): I = dacitic to rhyolitic ignimbrite, BV = basal vitrophyre, T = unwelded tuff, VB = volcanic breccia. Min (interpreted mineralogic carrier): M = magnetite, H = hematite, B = coexisting and colinear magnetite and hematite components. N/n/v: (N) number of specimens measured/(n) number of specimens used in site mean calculation/(v) number of directions in (n) that are defined by vectors, rather than great circles. Dg/Ig: declination/inclination in geographic coordinates. Ds/Is: declination/inclination in tilt-corrected coordinates. α_{95}: the semi-angle of the 95% cone of confidence about the site mean direction. k: *Fisher* [1953] precision parameter. Strike/Dip: Bedding orientation determined from field observations. AMS: Interpreted nature of bedding attitude (P = primary, S = secondary) from anisotropy of magnetic susceptibility data. Slat/Slon: site latitude/longitude. $Plat_1/Plon_1$: virtual geomagnetic pole latitude/longitude determined from raw tilt-corrections. $Plat_2/Plon_2$: virtual geomagnetic pole latitude/longitude determined from AMS interpreted tilt-corrections ($Plat_1/Plon_1 = Plat_2/Plon_2$ when the bedding attitude is interpreted to be secondary). A_{95}: the semi-angle of the 95% cone of confidence about the virtual geomagnetic pole. Rejected sites are italicized. Merged sites were calculated by combining data at the sample level from multiple sites that were interpreted to represent a single cooling unit. Magnetization directions were corrected for anisotropy by applying the inverse ATRM tensor, or by assuming $P_{TRM} \approx P_{AMS}^2$ (see text) and $\tan I_i = \tan I_c/P_{TRM}$. Di/Ii: initial declination/inclination. Dc/Ic: corrected declination/inclination.
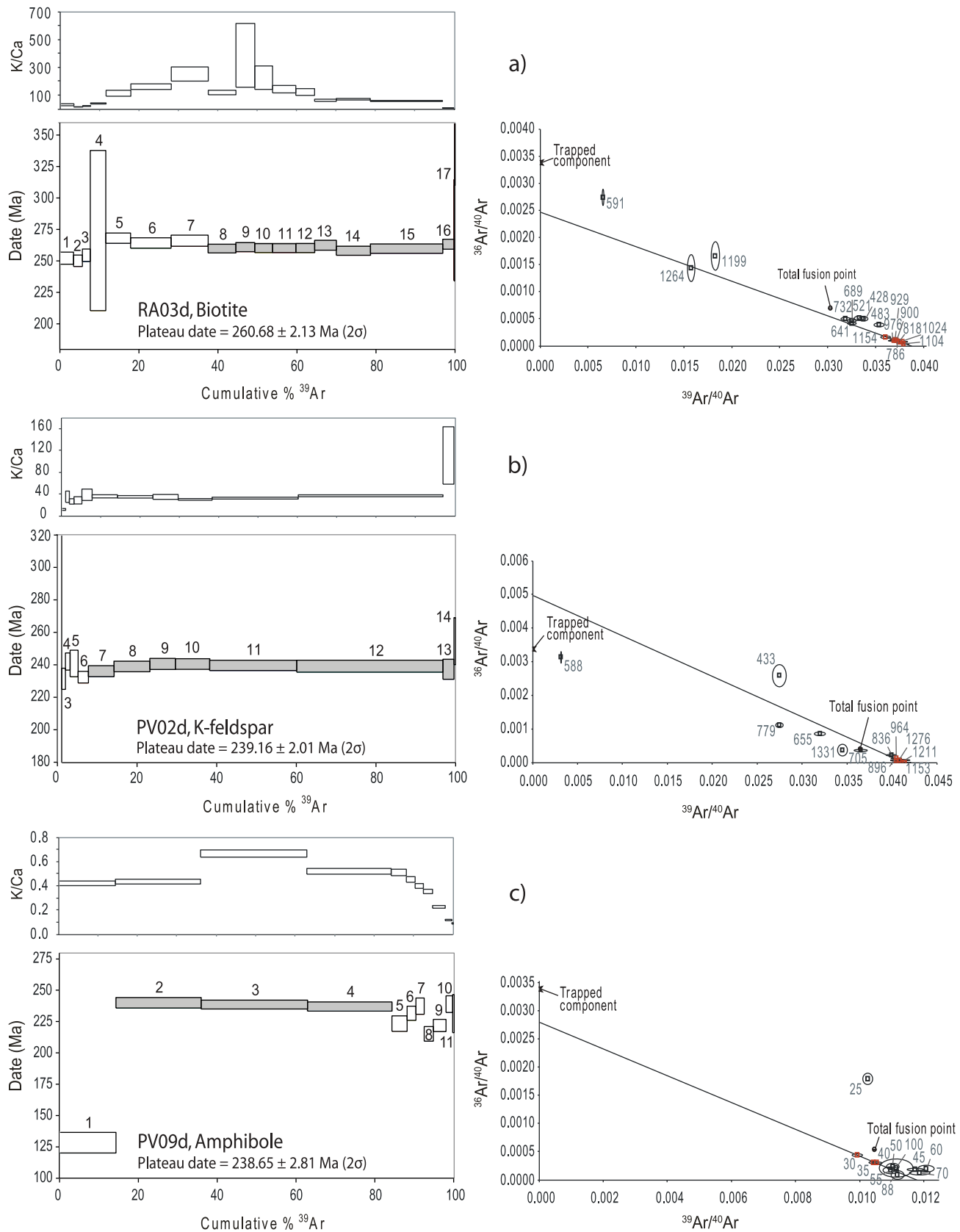
Figure 5

Hematite is assumed to contribute significantly to the AMS of the Puesto Viejo Group volcaniclastic rocks and to select Upper Choiyoi Group volcanic rocks where it dominates the NRM. Although crystallographic, strain, and grain-interaction effects all contribute to the low-field magnetic susceptibility of magnetite, it is the summation of weak shape-effects that commonly dominate the measured anisotropy [*Hrouda*, 1982; *Grégoire et al.*, 1998]. Inequant grains can become aligned during the emplacement of a rock body (via volcanic/fluvial flow) or by nucleation along preferred orientations in a pre-existing matrix, thus allowing the accessory magnetite to act as a proxy for bulk-rock petrofabric [*Le Pennec et al.*, 1998; *Pioli et al.*, 2008].

[28] Magnetic fabric studies conducted on ignimbrites have classically been used to study flow directions and emplacement mechanisms, but here we employ AMS as a tool to interpret our structural field-observations. Ignimbrite AMS is generally characterized by a well-defined, sub-horizontal magnetic foliation (plane common to K_{max} and K_{int}), perhaps imbricated so that the foliation plane dips "upcurrent" [*Ellwood*, 1982; *Incoronato et al.*, 1983; *Baer et al.*, 1997; *Palmer and MacDonald*, 1999]. Within the foliation plane, particle long-axes may be aligned parallel or perpendicular to the transport direction, according to the flow regime [*Khan*, 1962; *Tarling and Hrouda*, 1993; *Cagnoli and Tarling*, 1997; *Ort et al.*, 2003]. We postulate that structurally perturbed ignimbrites can potentially be discriminated from units emplaced on a pre-existing slope through a comparison of AMS characteristics and field-observations. For example, an ignimbrite that was emplaced on a horizontal surface and subsequently tilted would not necessarily yield a magnetic lineation or imbrication with any correlation to the (younger) structural attitude. Indeed, the lineation and/or imbrication may be suppressed if local flow was not organized by a sloping surface. Conversely, in an ignimbrite emplaced on a pre-existing slope, K_{max} and K_{int} may correspond with the strike and dip directions of the slope, and an imbrication may leave the magnetic foliation shallower or steeper than the field-observed dip, depending on the relationship between flow direction and slope. Obviously, these expectations are qualitative in nature and may be rendered invalid by complexities in mineralogy or flow emplacement, or by later deformation. For this reason, we treat the AMS results as an interpretive tool, rather than a structural data set. In the following, we present two applications of this method to the current study; a discussion of the remaining data (Table 4) can be found in the auxiliary material.

[29] In Cuesta de los Terneros, a thick sequence of Puesto Viejo Group sedimentary and volcanic rocks constitute a narrow WNW-ESE oriented plateau. Along the eastern margin of this plateau, the beds are tilted 22° to the west. This structural attitude is reflected in the highly consistent AMS of ignimbrite samples from this sequence (Table 4): a well-defined magnetic foliation is parallel to the bedding plane (Figure 10a). No statistically distinct (95% confidence) magnetic lineation is observed. These characteristics suggest that the structural attitude of this sequence is secondary.

[30] In the Atuel River Canyon, a sequence of Upper Choiyoi Group volcanic rocks dips 13° to the southeast. AMS data from samples of these volcanic rocks (Table 4) show a well-defined, sub-horizontal magnetic foliation and a subsidiary, but statistically significant (95% confidence) magnetic lineation (Figure 10b). Although dipping to the southeast, the magnetic foliation plane is shallower than the field-estimated bedding attitude, possibly due to grain imbrication. The magnetic lineation is parallel to the strike of the bedding plane. This combination of characteristics is consistent with well-organized pyroclastic flow, directed parallel to the dip direction of the beds. We therefore interpret the structural attitude of this sequence to be primary (i.e., the dip pre-dates the volcanic rocks).

7.2. Other Magnetic Fabrics

[31] As aforementioned, we have assumed that the low-field AMS is controlled largely by accessory magnetite (with an important contribution from hematite in select sites) and that the resulting magnetic fabrics are broadly representative of the bulk petrofabric of the rock. To validate these assumptions, we conducted additional magnetic anisotropy analyses on a select set of samples (Table 5). The anisotropy of anhysteric remanence (AARM), thermal remanence (ATRM), and high-field susceptibility (HF-AMS) target more specific mineral constituents, allowing a comparison of magnetic sub-fabrics and a means of determining the degree of alignment among different minerals. The AARM, ATRM, and HF-AMS results (discussed in the auxiliary material) are in general agreement with the AMS data and reinforce the supposition that the AMS is controlled by magnetite, but is broadly representative of other mineral subfabrics.

8. Directional Analysis

8.1. Puesto Viejo Group

[32] Tilt-corrections are applied to the Puesto Viejo Group ChRMs according to both raw field observations (hereafter "raw corrections") and AMS interpretations (hereafter "AMS corrections"). Results of the bootstrap foldtest [*Tauxe and Watson*, 1994] suggest that the ChRMs were acquired prior to tilting, as directional co-axiality peaks at 99% untilting (95% confidence bounds: 72–125%) for the raw corrections (Figure 11, top). The AMS corrections similarly result in peak co-axiality at 112% untilting (95% confidence bounds: 89–135%). Because the foldtest is designed to detect relative improvements in directional clustering, a comparison of the optimal untilting values from the raw and AMS corrections can be misleading. For example, the

Figure 5. Example ^{40}Ar-^{39}Ar results. Figures 5a–5c (left) show K-Ca ratios (top) and calculated date (bottom) as a function of released ^{39}Ar during progressive stepwise heating (bars are plotted at 2σ error). The numbers in the date spectrum plot indicate the heating step; the filled bars were used in the calculation of the plateau date. Figures 5a–5c (right) show inverse isochron diagrams. Red symbols indicate the steps used in the inverse isochron calculation. Results from (a) an Upper Choiyoi Group ignimbrite, (b) a Puesto Viejo Group ignimbrite, and (c) a Puesto Viejo Group basalt. See the auxiliary material for the complete results.
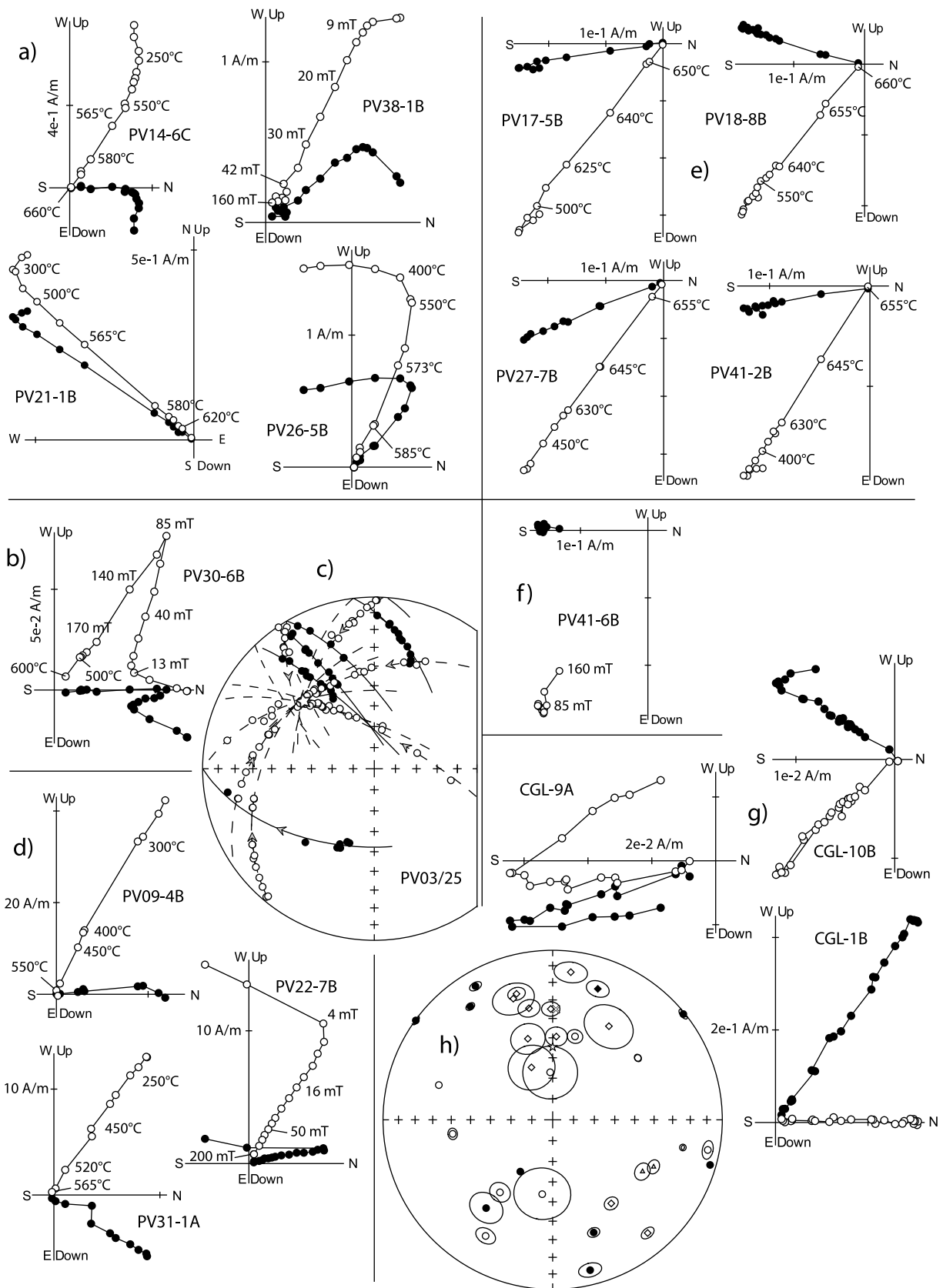
Figure 6

resultant vector length of the ChRMs, R (calculated after the directions are converted to a common polarity), is slightly higher at 100% untilting when the AMS corrections are used, even though the raw corrections reach peak co-axiality at 99% untilting (Figure 11, top). The decreased width of the 95% confidence bounds on the optimal untilting value of the AMS corrections also suggests they offer an improvement over the raw corrections.

[33] In either case, after tilt-corrections are applied the ChRMs from the volcanic and volcaniclastic rock subsets remain statistically distinct (95% confidence), implying that they do not belong to a common distribution. Re-applying the foldtest to these individual ChRM subsets, the volcanic rock directions again yield a positive result: optimal untilting at 102% (95% confidence bounds: 70–134%, raw corrections) or 118% (95% confidence bounds: 94–142%, AMS corrections), but the test of the volcaniclastic rock ChRMs yields an inconclusive result: optimal untilting at 64% (95% confidence bounds: 31–97%, raw corrections) or 48% (95% confidence bounds: 8–89%, AMS corrections). Using either set of tilt-corrections, both the volcanic and volcaniclastic rock ChRM subsets independently pass the bootstrap reversal test, indicating that their normal and reverse components have a common origin, and that additional magnetizations have been effectively removed. After tilt-correcting locally faulted sites in the Valle Grande area, additional volcanic rock site-mean directions from neighboring sites are found to be statistically indistinct (95% confidence), and are merged to prevent a weighting bias (Table 1).

[34] In addition to the application already discussed, magnetic anisotropy measurements can be used to correct for bias in a magnetization direction due to sedimentary flattening (pertinent to DRMs) or magnetic refraction (where a thermal remanent magnetization (TRM) is deflected from the ambient magnetic field direction due to shape effects). To test for such bias, ATRM measurements were made on select samples from sites with the highest degree of AMS (Table 5; auxiliary material). The results indicate that a minor bias is present in the volcanic rock samples with a relatively high degree of AMS (P ≥ 1.02), but that the majority of the volcanic rock ChRMs have a negligible error (≤1°). For the select sites that we measured ATRM (those that had the highest degree of AMS), we corrected the site mean directions with the inverse ATRM tensor (Table 1).

[35] ATRM measurements on select volcaniclastic rock samples reveal a more substantial shallow inclination bias of ∼5.5°. However, correction of the volcaniclastic rock directions is not straightforward because the ChRM is likely a DRM, and the intrinsic particle anisotropy (α) is not known.

Moreover, the larger collection of AMS measurements cannot be used to determine the prevalence of any shallow inclination bias because the AMS is likely controlled by trace amounts of magnetite, whereas the ChRM is carried by hematite. Some assumptions are therefore necessary. If we assume that the ChRM is a DRM (discussed below) and all the volcaniclastic rocks have experienced the same degree of sedimentary flattening, we may apply a blanket correction following the relationship of *King* [1955]: tan (I_o) = f tan (I_f), where f is the "flattening" coefficient, and I_o and I_f are the observed and true field inclinations, respectively. The value of f can be calculated from the ATRM data if we further assume that $\alpha = \infty$, in which case the remanence (ATRM) ellipsoid is identical to the DRM ellipsoid [*Jackson*, 1991]. Following this assumption, the ATRM results indicate that the volcaniclastic rocks have been flattened by $f = 0.8$. In reality, α is likely to be finite, so this is a minimum estimate of shallowing (the true value of f is likely lower). A more accurate value of f may be calculated if we assume that the difference in the mean ChRM directions of the volcanic and volcaniclastic rocks is due to inclination shallowing of the latter. The mean inclinations of these data sets can be brought into agreement by applying an inclination correction of $f = 0.71$ to the volcaniclastic rock ChRMs. For reference, f values from hematite-bearing sedimentary rocks have been observed to range from 0.40 to 0.83 [*Bilardello and Kodama*, 2010]. Unfortunately, we do not have a sufficient number of sites from the volcaniclastic rocks to independently estimate the true inclination bias (as per the technique of *Tauxe et al.* [2008]), so the validity of the $f = 0.71$ correction is dependent on the assumption that the mean ChRM direction of the volcanic rocks is well-determined and that it shares a common true direction with the mean ChRM of the volcaniclastic rocks.

[36] After anisotropy correction, the paleomagnetic pole derived from the raw tilt-corrected volcanic rock ChRMs is: 77.8°S, 322.4°E, A_{95}: 7.8°; if the AMS-interpreted tilt-corrections are used, the pole is: 76.7°S, 312.4°E, A_{95}: 7.3° (Table 1). For reference, the pole position previously determined from Puesto Viejo Group volcanic rocks by *Valencio et al.* [1975] was: 76°S, 236°E, A_{95}: 18°. The paleomagnetic pole derived from the $f = 0.8$ corrected volcaniclastic rock ChRMs is: 81.2°S, 301.0°E, A_{95}: 4.8° (100% untilted, AMS tilt-corrections). Using the larger anisotropy correction ($f = 0.71$) the paleomagnetic pole is: 77.9°S, 297.8°E, A_{95}: 4.6° (100% untilted, AMS tilt-corrections) (Table 1). If the volcaniclastic rock ChRMs are not corrected for anisotropy, the tilt-corrected paleopole is sub-parallel to the rotation axis (using either set of tilt-corrections).

Figure 6. Characteristic demagnetization behavior of samples from the Puesto Viejo Group. All directions are presented in geographic coordinates. In the orthogonal vector diagrams the solid (open) symbols are projections onto the horizontal (vertical) plane. For the stereonets the solid (open) symbols are projections onto the lower (upper) hemisphere. (a) Typical ignimbrite samples. (b) Ignimbrite sample showing the high-stability C component. (c) Example of converging great circle demagnetization trajectories; the star represents the common high-stability component. (d) Typical basalt samples. (e) Typical volcaniclastic rock samples. (f) AF demagnetization of a volcaniclastic sample. (g) Typical conglomerate clast samples. (h) Sample-level component directions from the conglomerate clast samples: diamonds (circles) denote the low- (high-) temperature components. The triangles represent the high-temperature components of two independent samples collected from the same clast, indicating that the randomness of the high-temperature component is not due to viscous behavior. The "x" (star) denotes the direction of the present-day field (present-day dipole).
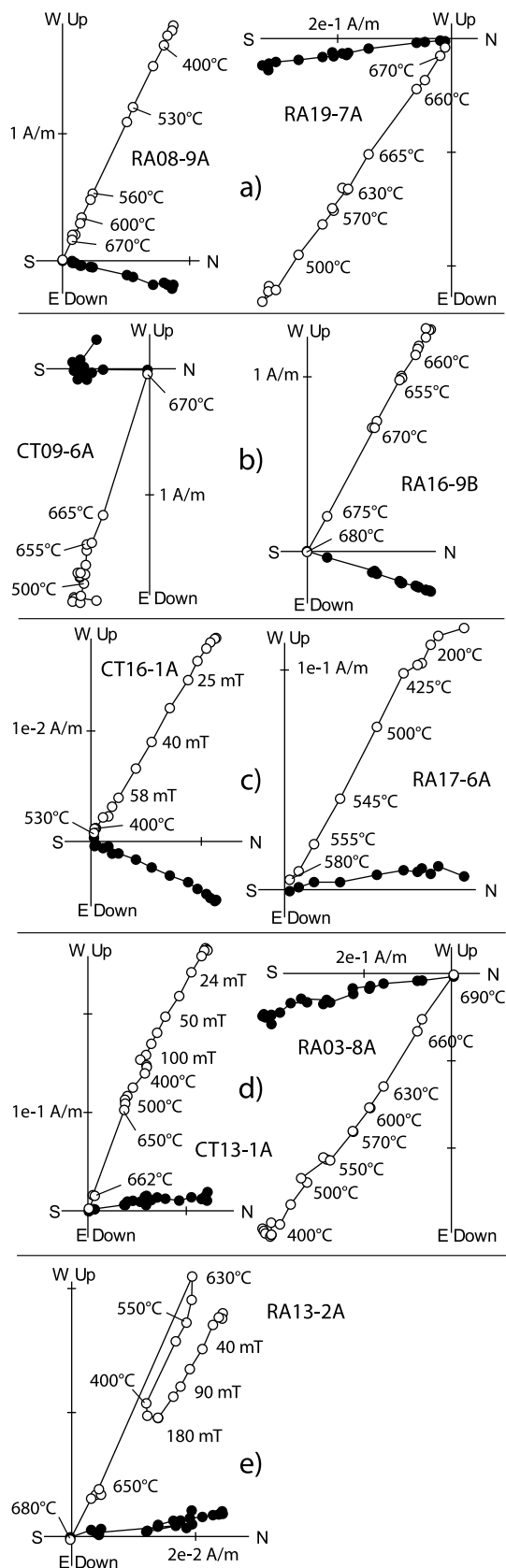
8.2. Upper Choiyoi Group

[37] The bootstrap foldtest of the Upper Choiyoi Group ChRMs is inconclusive if the raw tilt-corrections are used: optimal untilting occurs at 42% (95% confidence bounds: 22–62%), but positive if the AMS tilt-corrections are used: optimal untilting at 101% (95% confidence bounds: 75–126%) (Figure 11, bottom). The ChRMs pass the bootstrap reversal test after applying either set of tilt-corrections. A select set of ATRM measurements on samples with the highest degree of AMS (Table 5) again indicate that a directional bias is present in the most anisotropic samples. Unfortunately, ATRM measurements were not made on all Upper Choiyoi Group sites that may be affected by such a bias (sites with P (of AMS) ≥ 1.02), but the larger collection of AMS results may be utilized because they convey the bulk anisotropy of the remanence carrying mineral in these rocks (magnetite). The FORC diagrams indicate that single-domain (SD) magnetite is not dominant in the Upper Choiyoi Group volcanic rocks, and the AARM measurements confirm that SD grains do not noticeably contribute to the AMS (see the auxiliary material). Given this, we adopt the theoretical relationship $P_{TRM} \approx P_{AMS}^2$, which *Cogné* [1987] has shown to be a reasonable approximation where the AMS is controlled by MD magnetite. Because the majority of the Upper Choiyoi Group AMS ellipsoids are oblate with a sub-vertical K_{min}, we further simplify the anisotropy corrections by assuming that P (of AMS) describes a pure, horizontal foliation. ChRMs carried solely by hematite are not corrected, because its anisotropy is unknown. The resulting corrections are small; 10 sites are corrected by this method, and the average change in inclination is 1.8° (Table 2).

[38] The mean directions from the different remanence carriers are statistically indistinguishable (95% confidence) after anisotropy- and tilt-correction. The combined results yield the paleomagnetic pole: 73.7°S, 315.6°E, A_{95}: 4.1° (AMS tilt-corrections). If the raw tilt-corrections are used the pole is: 81.0°S, 340.2°E, A_{95}: 4.4°.

9. Discussion

9.1. Interpretation of Geochronology Results

[39] Our new Upper Choiyoi Group SHRIMP U-Pb zircon date of 263.5 ± 2.0 Ma (sample "PV01d") is in agreement with the SHRIMP U-Pb zircon date determined for the Agua

Figure 7. Characteristic demagnetization behavior of samples from the Upper Choiyoi Group. All directions are presented in geographic coordinates. In the orthogonal vector diagrams the solid (open) symbols are projections onto the horizontal (vertical) plane. The illustrations are grouped according to the interpreted remanence carrier(s), as determined from demagnetization behavior and rock-magnetic experiments: (a) Two remanence carriers (magnetite and hematite), with parallel magnetization directions. (b) Remanence carried by hematite only. (c) Remanence carrier by magnetite only. (d) Two remanence carriers (magnetite and hematite) with statistically distinct (95% confidence) magnetization directions. (e) Example of rare, antipodal high-temperature components of magnetization, speculatively attributed to self-reversal.
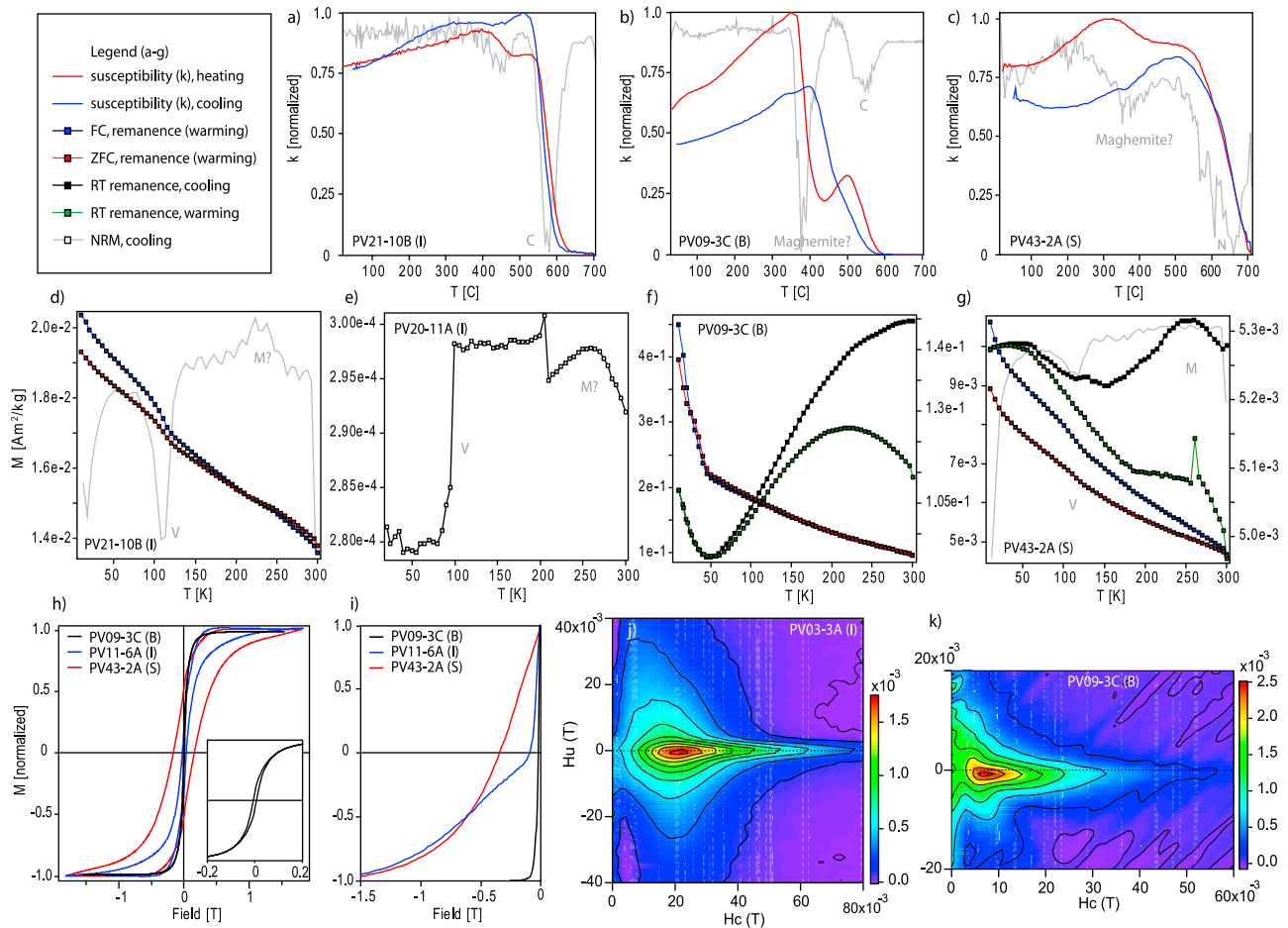
Figure 8. Rock magnetic experiments on Puesto Viejo Group samples. The lithology of the sample is denoted by the letter after the sample name: I = ignimbrite, B = basalt, S = volcaniclastic rock. (a–c) Thermomagnetic analysis (κ versus T). The gray line in these plots shows the first derivative of the heating curve. Interpreted magnetic critical points are labeled C (Curie) and N (Néel) temperatures. (d–g) Low-temperature remanence experiments. FC = field cooled, ZFC = zero field cooled. RT = isothermal remanent magnetization imparted at room temperature, NRM = natural remanent magnetization. The gray line in these plots shows the first derivative of the FC curve. Interpreted magnetic transitions are labeled V (Verwey) and M (Morin). (h) Hysteresis loops of characteristic samples after correction for paramagnetism. The inset shows the low-field behavior of sample PV09–3C. (i) Back-field curves for samples from Figure 8h. (j–k) Characteristic first-order reversal curves (FORC) for ignimbrite and basalt samples. A smoothing factor of 3 was applied to the FORC diagrams.

de los Burros Fm. (260.7 ± 2.1 Ma) by *Rocha-Campos et al.* [2011]. The comparable [40]Ar-[39]Ar date of 260.68 ± 2.13 Ma from sample RA03d implies that the U-Pb zircon dates are close to the true eruptive age of the volcanic rocks.

[40] Unexpectedly, the SHRIMP U-Pb zircon dates from the Puesto Viejo Group yield mid-to-Late Permian age estimates that resemble those of the Upper Choiyoi Group (260.8 ± 3.2 Ma and 269.0 ± 3.2 Ma). These dates contradict the Early to Middle Triassic age assigned to the Puesto Viejo Group on the basis of the paleontological record. However, the presence of angular unconformities and locally thick sequences of clastic sedimentary rocks between the Upper Choiyoi Group and Puesto Viejo Group volcanic rocks supports the notion that these eruptive episodes are separated by a significant interval of time. We therefore postulate that the

dated zircons from the Puesto Viejo Group ignimbrites are xenocrysts from the underlying Permian rocks, assimilated during magma ascent and eruption. In support of this hypothesis, microscopic examination of Puesto Viejo Group volcanic rocks has revealed an association between zircons and lithic fragments, some of which appear to have undergone weathering (Figure 12). All zircons are zoned in an oscillatory fashion, and overgrown rims, as might occur during high grade metamorphism or during long residence time within a large magma chamber, were not observed. We speculate that the Puesto Viejo magma chamber was insufficiently volumetric to generate new zircon grains or overgrowths [*Watson*, 1996].

[41] The [40]Ar-[39]Ar plateau dates from the Puesto Viejo Group volcanic rocks range from 235.3 ± 2.3 Ma to 239.3 ±

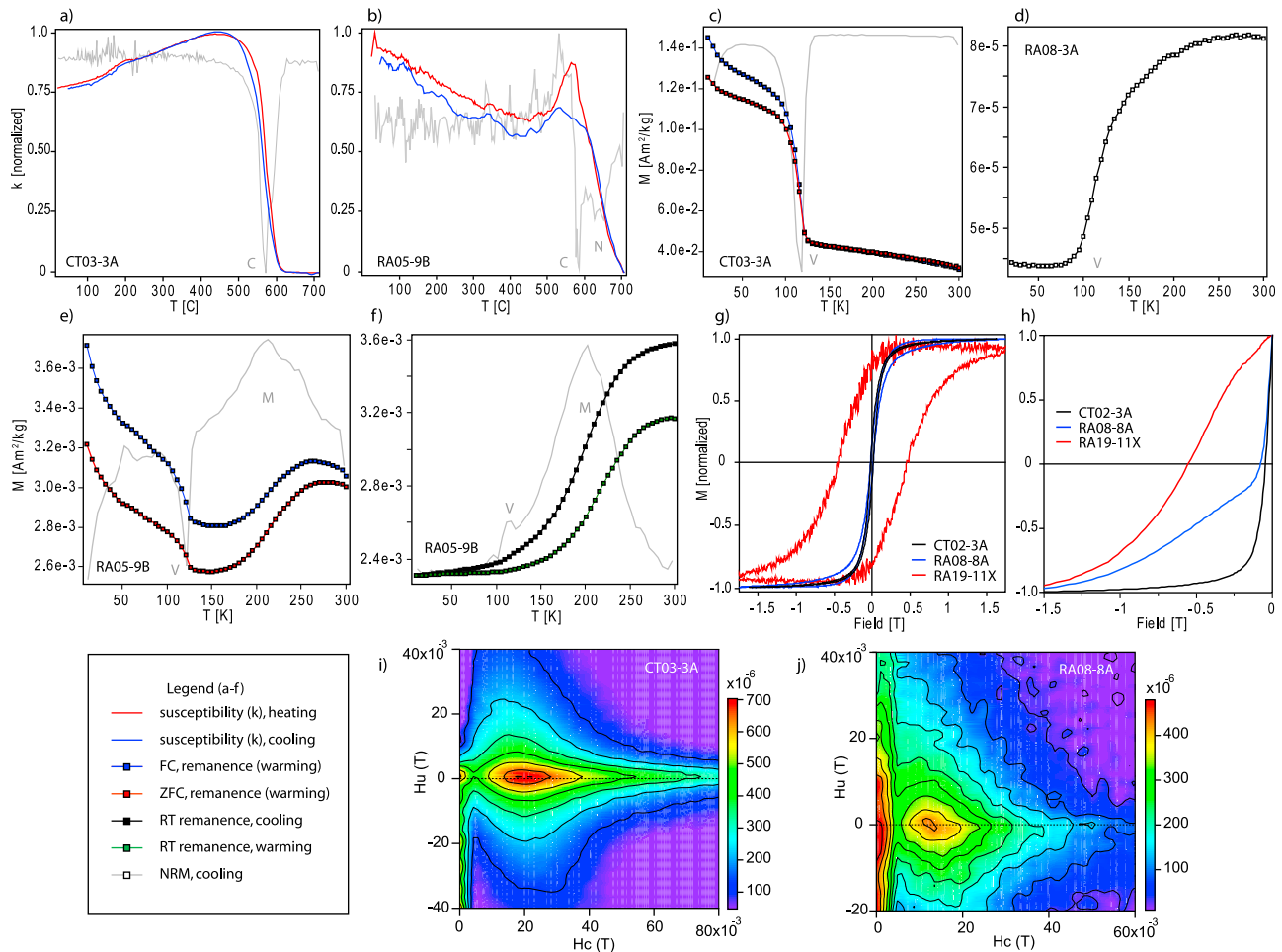**Figure 9.** Rock magnetic experiments on Upper Choiyoi Group samples. (a–b) Thermomagnetic analysis (κ versus T). The gray line shows the first derivative of the heating curve. Interpreted magnetic critical points are labeled C (Curie) and N (Néel) temperatures. (c–f) Low-temperature remanence experiments. FC = field cooled, ZFC = zero field cooled. RT = isothermal remanent magnetization imparted at room temperature, NRM = natural remanent magnetization. The gray line in Figures 9c and 9e shows the first derivative of the FC curve. The gray line in Figure 9f shows the first derivative of the RT cooling curve. Interpreted magnetic transitions are labeled: V (Verwey) and M (Morin). (g) Hysteresis loops of characteristic samples after correction for paramagnetism. (h) Back-field curves for samples from Figure 9g. (i–j) Characteristic first-order reversal curves (FORC). A smoothing factor of 3 was applied to the FORC diagrams.

3.2 Ma, in agreement with the recalculated K-Ar dates of *Valencio et al.* [1975]. We interpret these results to reflect the cooling ages of the volcanic rocks, corroborating a Middle Triassic age for Puesto Viejo Group volcanism. Late Permian and Early Triassic ^{40}Ar-^{39}Ar plateau dates from the Puesto Viejo Group volcaniclastic samples (248.6 ± 2.2 Ma and 254.7 ± 5.0 Ma) represent a minimum age for the Upper Choiyoi Group volcanic rocks, and a maximum age estimate for the overlying Puesto Viejo Group volcanic rocks. If the volcaniclastic rocks are constituted primarily by re-worked pyroclastic material from contemporaneous Puesto Viejo volcanism, these ages could be close to the true age of the volcaniclastic rocks.

[42] The ^{40}Ar-^{39}Ar plateau date of 239.5 ± 7.0 Ma from Upper Choiyoi Group sample CCH is attributed to thermal resetting during Middle Triassic volcanism/deformation, as it is proximal to Puesto Viejo Group volcanic rocks and a major post-SROP normal fault. Sample "PV01d-2" was collected from the Upper Choiyoi Group, approximately 10 km to the southeast of sample CCH, along the same major normal fault. It has yielded an ^{40}Ar-^{39}Ar plateau date of 255.7 ± 2.2 Ma that may represent a cooling age from late Upper Choiyoi volcanism (i.e., Cerro Carrizalito Fm.), or partial thermal resetting of an older age during Triassic volcanism/deformation.

[43] The Late Triassic and Early Cretaceous whole-rock ^{40}Ar-^{39}Ar dates from Puesto Viejo Group ignimbrites are confounding, as no record of post-Middle Triassic volcanism has been documented in this region. However, we note that the date-spectra of these results are discordant (weighted-

Table 4. AMS Results[a]

Site	N	Km	L	F	P	T	K1 Dec	K1 Inc	K3 Dec	K3 Inc
				Puesto Viejo Group						
Cuesta de los Terneros										
PV38	6	4.12E-03	1.002	1.019	1.022	0.780	327.7	0.8	224.3	86.4
PV39	6	2.92E-03	1.002	1.014	1.016	0.770	29.5	4.5	232.0	85.1
PV22	5	7.35E-02	1.004	1.007	1.011	0.267	168.2	8.7	52.9	70.2
PV20	12	6.21E-03	1.001	1.040	1.040	0.952	203.4	7.4	94.2	68.5
PV21	13	1.66E-03	1.005	1.050	1.056	0.804	304.1	19.1	100.6	69.3
PV24	10	3.53E-03	1.002	1.019	1.021	0.823	260.1	15.5	115.3	71.3
PV03	18	7.52E-03	1.001	1.044	1.044	0.965	297.2	18.3	94.7	70.3
PV26	13	6.33E-04	1.001	1.009	1.010	0.717	355.7	12.8	122.4	69.2
Atuel River area										
PV37	5	9.06E-05	1.002	1.007	1.008	0.615	206.3	15.5	54.7	72.5
PV36	7	8.77E-05	1.006	1.013	1.020	0.335	130.8	2.8	228.5	70.0
PV34	6	2.84E-05	1.010	1.028	1.037	0.477	314.8	15.4	95.6	70.4
PV33	5	5.65E-05	1.005	1.012	1.017	0.404	339.5	11.3	130.0	77.1
PV32	5	2.08E-05	1.017	1.002	1.019	−0.804	332.8	10.4	198.0	75.4
PV16	5	1.67E-04	1.001	1.009	1.010	0.745	83.2	5.6	324.1	78.6
PV17	7	1.76E-04	1.002	1.006	1.008	0.547	264.1	8.2	128.3	78.7
PV18	5	1.78E-04	1.001	1.006	1.008	0.613	329.1	6.8	113.4	81.6
PV15	11	1.89E-04	1.000	1.002	1.002	0.669	100.7	10.5	256.3	78.4
Valle Grande area										
PV28	18	5.96E-05	1.002	1.000	1.002	−0.776	148.2	26.9	13.8	54.1
PV31	5	3.50E-02	1.006	1.020	1.026	0.550	86.6	22.5	291.3	65.5
PV09	9	2.80E-02	1.011	1.008	1.019	−0.181	132.7	3.3	248.1	82.3
PV40	6	1.55E-04	1.006	1.007	1.013	0.131	183.1	12.6	352.7	77.2
PV41	5	1.83E-04	1.005	1.011	1.016	0.355	187.2	2.2	290.9	80.8
PV42	5	1.66E-04	1.003	1.010	1.013	0.513	193.0	4.9	337.0	83.9
PV44	5	1.87E-04	1.004	1.022	1.025	0.716	186.4	6.6	339.6	82.6
Old Puesto area										
PV14	7	9.32E-04	1.001	1.013	1.015	0.836	137.4	4.3	333.2	85.5
PV11	9	9.44E-05	1.001	1.007	1.008	0.708	38.3	48.4	215.8	41.6
PV02	9	6.44E-04	1.001	1.003	1.004	0.535	23.4	36.3	220.9	52.4
Averaged results										
PV38-39	12	3.52E-03	1.001	1.017	1.018	0.887	351.6	2.3	227.9	85.8
PV03,20-26	66	3.70E-03	1.001	1.033	1.034	0.931	304.3	18.6	99.9	69.7
PV32-37	28	5.58E-05	1.008	1.011	1.019	0.193	326.2	9.0	120.9	80.1
PV15-18	28	1.80E-04	1.001	1.005	1.006	0.774	271.3	0.7	129.8	89.1
PV40-44	21	1.72E-04	1.004	1.013	1.017	0.518	186.2	6.5	332.6	82.2
PV02,11	18	3.30E-04	1.001	1.005	1.006	0.664	31.1	44.4	217.5	45.5
				Upper Choiyoi Group						
Cuesta de los Terneros										
CT03	7	2.78E-04	1.019	1.021	1.040	0.040	185.3	18.3	345.2	70.6
CT04	5	2.47E-03	1.005	1.004	1.001	−0.092	46.6	47.2	185.5	34.9
CT02	6	8.27E-03	1.004	1.005	1.092	0.024	118.7	18.6	258.3	66.2
CT13	5	8.28E-05	1.009	1.083	1.093	0.791	212.5	9.0	53.2	80.4
CT06	5	9.65E-05	1.006	1.030	1.036	0.678	209.9	2.4	79.9	86.2
CT05	5	1.21E-04	1.004	1.037	1.041	0.785	59.9	3.8	280.6	85.0
CT12	6	2.04E-05	1.004	1.002	1.006	−0.286	235.0	14.3	347.5	56.3
CT09	5	6.22E-05	1.004	1.081	1.086	0.890	206.5	7.4	0.4	81.8
CT07	9	1.29E-04	1.004	1.062	1.067	0.862	163.3	3.8	26.2	84.9
CT17	7	3.80E-05	1.001	1.001	1.002	0.196	50.7	6.2	299.8	73.1
CT18	7	8.01E-05	1.004	1.005	1.009	0.106	273.7	13.2	172.2	40.3
CT14	8	1.40E-04	1.006	1.002	1.008	−0.529	298.7	6.7	195.1	63.4
Atuel River area										
RA08	6	1.31E-04	1.002	1.011	1.013	0.631	94.7	3.4	317.9	85.3
RA09	6	2.25E-04	1.003	1.017	1.021	0.674	253.9	5.2	94.7	84.4
RA06	5	2.81E-05	1.006	1.004	1.008	0.077	37.4	4.3	291.3	75.0
RA07	6	5.56E-05	1.002	1.005	1.007	0.488	162.3	9.5	296.4	76.5
RA20	7	4.25E-05	1.009	1.043	1.053	0.634	40.9	12.7	245.8	76.0
Valle Grande area										
RA17	5	1.65E-04	1.005	1.022	1.027	0.655	271.9	1.2	41.7	88.1
RA16	7	2.30E-05	1.007	1.036	1.043	0.679	206.9	5.9	16.1	84.0
RA14	6	4.77E-05	1.003	1.028	1.032	0.790	64.0	8.7	285.0	78.6
RA13	5	4.97E-05	1.002	1.019	1.021	0.789	50.5	2.0	305.8	82.1
RA12	7	3.73E-05	1.001	1.001	1.001	−0.459	231.3	48.9	137.1	3.6
RA11	6	3.64E-05	1.001	1.001	1.001	0.362	185.6	8.7	282.1	36.5
RA18	6	3.32E-05	1.006	1.016	1.023	0.425	38.2	8.2	274.9	75.3
RA19	8	7.03E-05	1.025	1.080	1.108	0.508	65.7	1.1	328.6	81.3
RA10	6	1.16E-04	1.008	1.038	1.046	0.656	29.6	14.1	192.4	75.3

Table 4. (continued)

Site	N	Km	L	F	P	T	K1 Dec	K1 Inc	K3 Dec	K3 Inc
Rio Seco los Leones										
SL01	5	2.97E-05	1.001	1.001	1.001	0.046	158.8	4.7	67.4	16.7
SL03	7	1.84E-05	1.001	1.032	1.039	0.646	215.5	26.7	46.9	62.9
SL02	5	8.74E-05	1.001	1.003	1.004	0.439	333.7	4.6	79.5	73.4
SL04	6	3.31E-05	1.001	1.002	1.004	0.398	274.0	0.5	181.2	79.6
Averaged Results										
RA08-09	12	1.78E-04	1.003	1.014	1.017	0.680	261.6	2.3	61.1	87.6
RA06-07	11	4.08E-05	1.002	1.005	1.007	0.551	200.0	0.8	293.3	75.9
RA13-19	37	6.17E-05	1.008	1.037	1.045	0.654	58.7	1.2	319.1	83.0

[a]AMS: anisotropy of magnetic susceptibility. N: number of specimens. Km: average bulk volume susceptibility in SI units. L (lineation): τ_{max}/τ_{int}. F (foliation): τ_{int}/τ_{min}. P (degree of anisotropy): τ_{max}/τ_{min}. T (shape factor; *Jelinek* [1981]): $2(\ln(\tau_{int}/\tau_{min})/\ln(\tau_{max}/\tau_{min}))-1$. K1 Dec/Inc: declination/inclination of site mean K_{max}. K3 Dec/Inc: declination/inclination of site mean K_{min}. Averaged results are combined sample-level data from adjacent sites with the same structural orientation and highly similar AMS.

mean dates), indicating that the isotopic system of these samples has likely been disturbed. Notably, the ^{40}Ar-^{36}Ar ratio determined from sample PV30d is 235.7 ± 25.9, which is statistically distinct (95% confidence) from the known atmospheric value of ~298. Thus, we regard these whole-rock dates as unrepresentative of the emplacement age of these rocks.

[44] With regard to these new results, we assign the sampled Upper Choiyoi Group (Agua de los Burros Fm.) a best-estimated age of ca. 264 Ma (Capitanian). The volcanic rocks of the Puesto Viejo Group yield consistent Middle Triassic ^{40}Ar-^{39}Ar plateau dates with an average of ca. 238 Ma, but the mean age of the group may be older, as reflected by the maximum ages of the volcaniclastic rocks and the identification of Early Triassic fossils. We therefore assign the
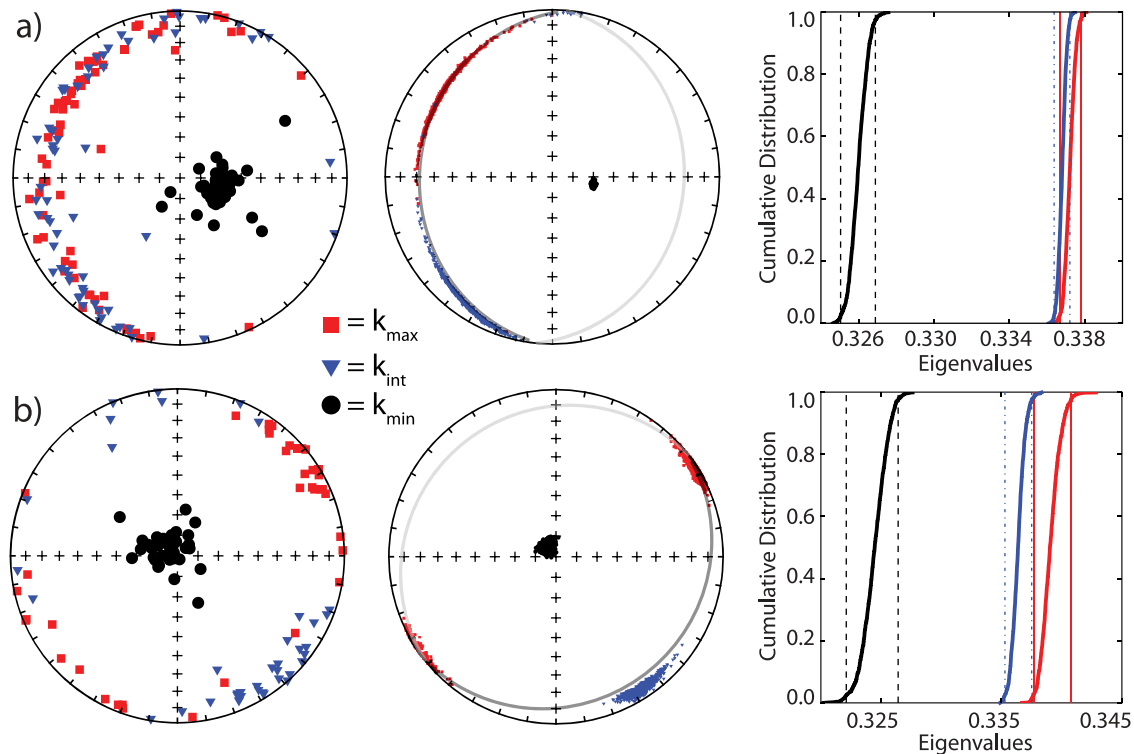
Figure 10. Example anisotropy of magnetic susceptibility (AMS) results from (a) sites PV03, 20–26 and (b) sites RA13–19. Results are presented in geographic coordinates. All symbols are projections onto the lower hemisphere. (left) The raw sample-level data. (middle) 1000 bootstrapped eigenvectors [*Constable and Tauxe*, 1990] of the raw data. The gray lines depict the bedding attitude of the sites, as estimated from field-observations; the darker (lighter) line is a projection onto the lower (upper) hemisphere. (right) The relative eigenvalues (as cumulative distribution functions) associated with the eigenvectors: red = maximum (τ_{max}), blue = intermediate (τ_{int}), black = minimum (τ_{min}). The vertical dashed lines are the 95% confidence bounds on the eigenvalue estimates.

Table 5. AARM, ATRM, and HF-AMS Results[a]

Site	N	Mrm or Km	L	F	P	T	K1 Dec	K1 Inc	K3 Dec	K3 Inc
AARM										
PV38-39	13	1.87E+00	1.010	1.172	1.183	0.884	33.5	1.2	280.9	86.8
PV22	5	2.63E+00	1.002	1.014	1.016	0.695	13.8	26.5	209.9	62.6
PV20-24	17	1.65E+00	1.013	1.099	1.113	0.767	279.2	17.4	85.6	72.1
PV28	8	1.51E-02	1.008	1.006	1.014	−0.1	211.4	46	32.1	44
RA19	8	5.31E-01	1.079	1.171	1.264	0.35	64.2	4.4	310.4	79.1
ATRM										
PV38-39	7	1.89E+00	1.061	1.077	1.142	0.116	134.3	10.4	299.2	79.2
PV20-24	14	2.43E+00	1.034	1.095	1.132	0.462	224.8	7.1	118.6	65.8
PV40-44	9	1.82E-01	1.058	1.153	1.22	0.432	179.4	9.6	334.5	79.4
RA19	7	2.70E+00	1.112	1.206	1.341	0.276	134.3	2.8	343.1	86.8
HF-AMS										
PV38-39	7	1.05E-08	1.020	1.065	1.086	0.515	129.5	79	35.2	0.8
PV20-24	14	4.73E-09	1.295	1.151	1.49	−0.3	47.7	73.7	142.7	1.5
PV03	4	6.91E-10	-	-	-	-	233.5	24.6	136.4	15.1
PV28	7	7.46E-09	1.089	1.038	1.131	−0.39	9.8	58.3	277	1.7
RA19	7	2.22E-08	1.083	1.067	1.156	−0.1	114.8	59.3	16.5	4.9

[a]AARM: anisotropy of anhysteretic remanent magnetization. ATRM: anisotropy of thermal remanent magnetization. HF-AMS: anisotropy of high-field magnetic susceptibility. N: number of specimens. Mrm: average sample remanence in A/m. Km: average bulk high-field magnetic susceptibility in m^3/kg. L (lineation): τ_{max}/τ_{int}. F (foliation): τ_{int}/τ_{min}. P (degree of anisotropy): τ_{max}/τ_{min}. T (shape factor; *Jelinek* [1981]): $2(\ln(\tau_{int}/\tau_{min})/\ln(\tau_{max}/\tau_{min})) - 1$. K1 Dec/Inc: declination/inclination of site mean K_{max}. K3 Dec/Inc: declination/inclination of site mean K_{min}.
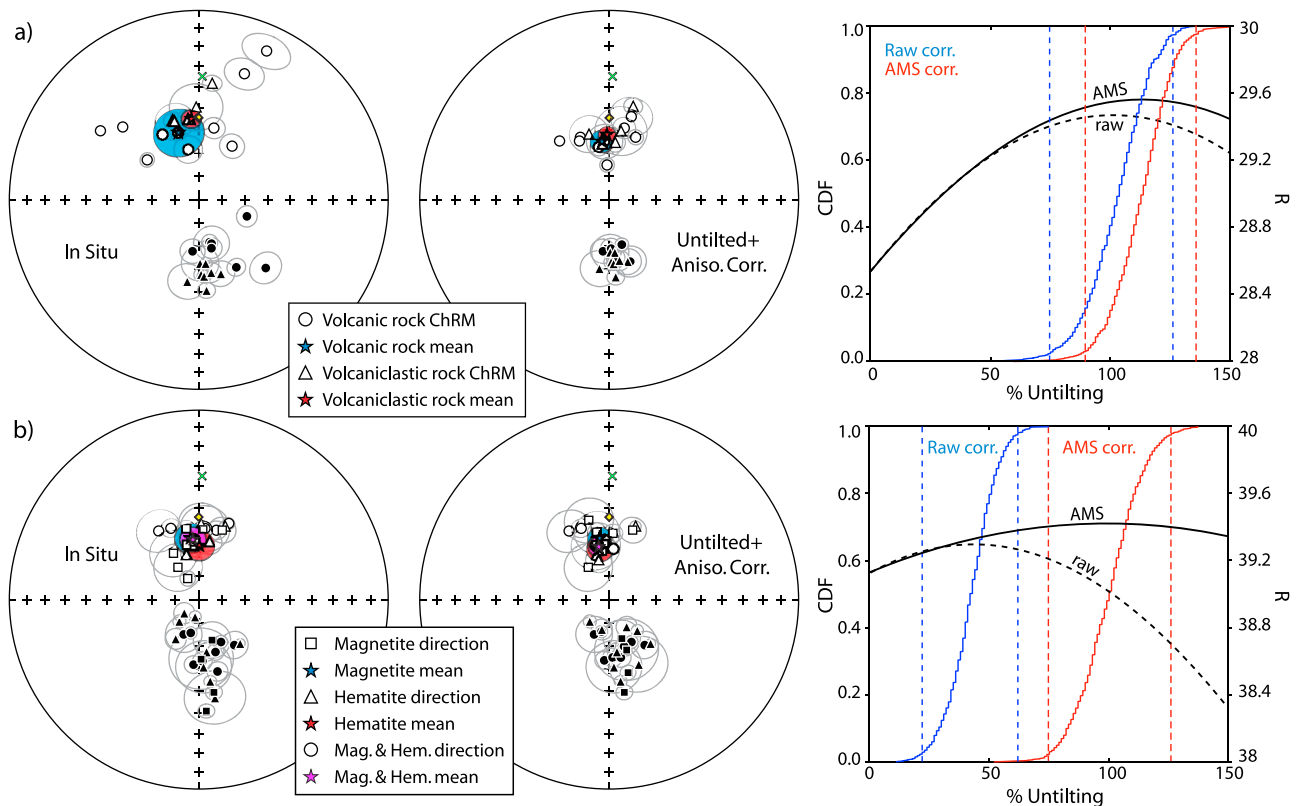
Figure 11. Site mean ChRM directions and foldtest results from (a) the Puesto Viejo Group and (b) the Upper Choiyoi Group. (left) The in situ site mean ChRM directions and group means with their associated α_{95} (projected cone of 95% confidence) The solid (open) symbols are projections onto the lower (upper) hemisphere. The green "x" (yellow diamond) denotes the direction of the present-day field (present-day dipole). (middle) The site mean ChRM directions and group means after 100% untilting (using the AMS-interpreted corrections) and correction for magnetic anisotropy. (right) The results of the bootstrap foldtest, using the raw tilt-corrections (blue cumulative distribution function and dashed black curve) and the AMS-interpreted tilt-corrections (red cumulative distribution function and solid black curve). The cumulative distribution functions reveal the location of optimal untilting (maximum magnetization direction co-axiality), with 95% confidence bounds (dashed vertical lines). The black curves show the change in total resultant vector length (R) of the magnetization direction population as a function of unfolding.
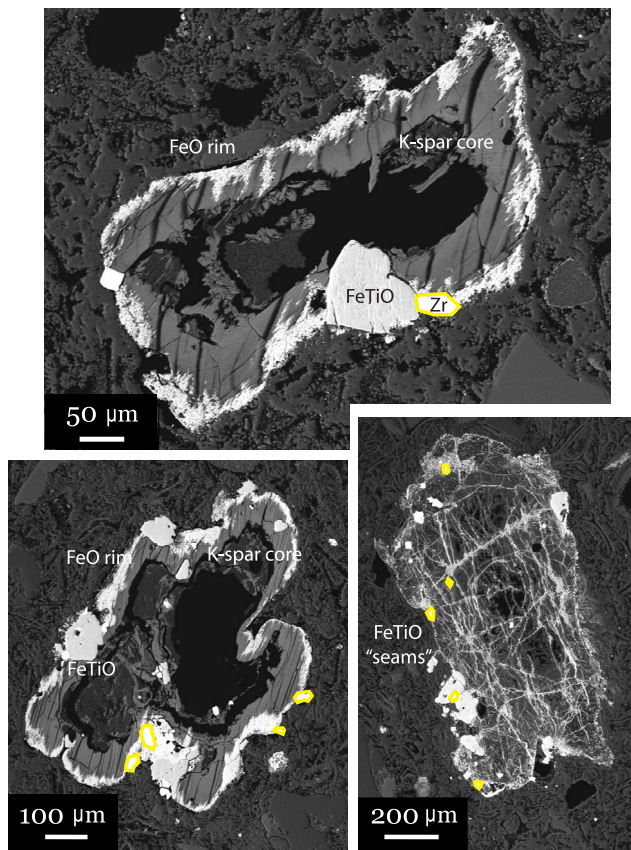
Figure 12. SEM photomicrographs of samples from the Puesto Viejo Group showing an association between zircons and lithic fragments. FeO = unidentified iron-oxide phase, FeTiO = unidentified iron-titanium oxide phase, K-spar = potassium feldspar, Zr = zircon (also highlighted in yellow).

Puesto Viejo Group an Early to Middle Triassic (Olenekian-Anisian) age of ca. 245 Ma.

9.2. Interpretation of Paleomagnetic Results

[45] The positive foldtest of the Puesto Viejo Group volcanic rocks implies that their magnetization acquisition was very early, if not primary, because the Puesto Viejo Group was deformed by post-SROP regional tension that acted concurrently with Late Permian-Triassic volcanism. Post-Triassic deformation is not recognized in the SRB. A primary magnetization is further substantiated by the preservation of random directions in the clasts of the basal conglomerate of the Puesto Viejo Group, which indicates that no pervasive regional remagnetizations are manifest. The broad sample-level agreement in the magnetization direction of the magnetite and hematite components suggests their magnetization acquisition was near-synchronous, precluding the possibility that either developed as a later product of diagenesis/alteration. The positive reversal test indicates that magnetization acquisition among the Puesto Viejo Group sites must have been sufficiently distributed in time so as to sample both field polarities and average secular variation. The antipodal nature of the ChRM directions implies that they have been sufficiently separated from secondary overprints. We conclude that the ChRM of the Puesto Viejo Group

volcanic rocks is representative of the Early to Middle Triassic magnetic field, and we assign the associated paleopole the best-estimated age of 245 Ma.

[46] The nature and age of the Puesto Viejo Group volcaniclastic rock ChRM is more difficult to interpret. The inconclusive foldtest is inconsequential because the structural restorations are very minor. The reversal test is positive for both the uncorrected and the 100% untilted data sets. The absence of a prominent secondary magnetization in the basal conglomerate or proximal volcanic rocks suggests that a widespread chemical remagnetization (CRM) is unlikely, but the volcaniclastic rock ChRMs (without anisotropy correction) are close to the PDD, both before and after tilt-correction. If the pre-Middle Triassic ^{40}Ar-^{39}Ar dates from the volcaniclastic rock samples have escaped thermal reset-ting, the rocks would also have escaped thermal remagneti-zation, and the ChRM could be a primary DRM. We interpret the ChRM of the Puesto Viejo Group volcaniclastic rocks to be an early/primary DRM, but unrepresentative of the Early to Middle Triassic magnetic field due to a shallow inclination bias. However, it is important to reiterate that we cannot exclude the alternative possibility that the ChRM is a secondary CRM, in which case an inclination shallowing correction would not be applicable and the magnetization direction could be representative of a post-Middle Triassic magnetic field. In either case, this result is not useful for APWP construction.

[47] The positive foldtest of the Upper Choiyoi Group ChRM immediately precludes a post-Triassic remagnetiza-tion, as regional deformation ceased in the SRB prior to the end of the Triassic. The age of the ChRM can be further constrained by the AMS interpretations of the structural attitudes, which imply that the oldest Upper Choiyoi Group rocks have experienced greater deformation (see the auxiliary material). This contention agrees with independent structural observations that indicate that the SROP waned during emplacement of the Agua de los Burros Fm., implying that the oldest rocks were subjected to greater compression [*Kleiman and Japas*, 2009]. Therefore, acquisition of the Upper Choiyoi Group ChRM must have been very early, or primary, because deformation was partly contemporaneous with volcanism. An early/primary magnetization acquisition is again corroborated by a broad agreement in the magneti-zation direction of the magnetite and hematite components, and a positive reversal test implies that the ChRM is effec-tively purified of secondary magnetizations.

[48] We interpret the ChRM to be representative of the Late Permian magnetic field and assign the paleomagnetic pole the best-estimated age of 264 Ma, but again note the possible inclusion of some site-level data from younger Permian rocks (i.e., the Cerro Carizzalito Fm., ~252 Ma). We also note that the dual polarity of these results respects the presently known boundaries of the Kiaman Reversed Superchron (~318–265 Ma) [*Opdyke et al.*, 2000; *Gradstein et al.*, 2004].

9.3. Implications

[49] Since the late 1950s, it has been repeatedly demon-strated that the APWPs of Laurussia and Gondwana are disparate if a conventional "A-type" Pangea reconstruction is assumed [*Irving*, 2004]. For example, using the (A-type) reconstruction parameters and global paleomagnetic data
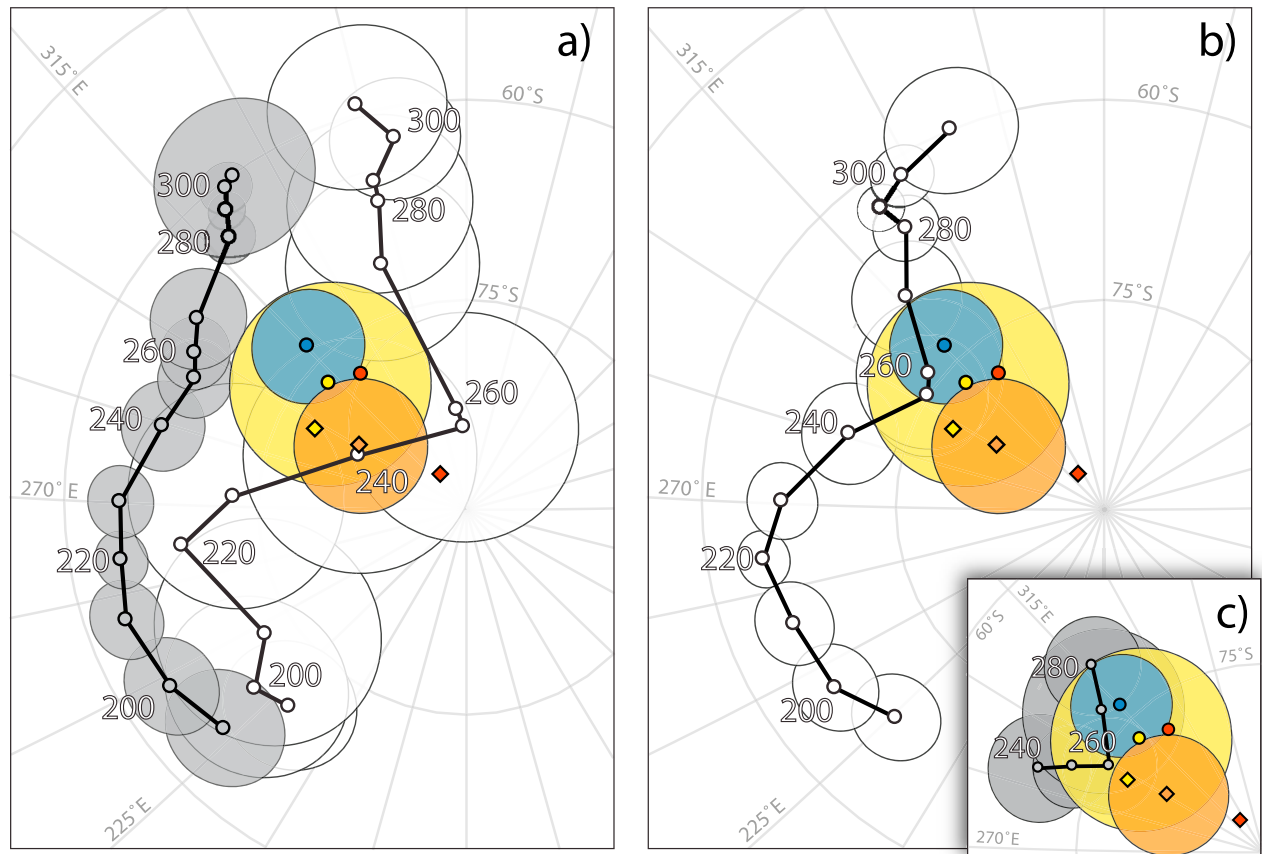
Figure 13. (a) Comparison of the new Puesto Viejo Group and Upper Choiyoi Group paleomagnetic poles with the APWPs of Laurussia (gray) and Gondwana (white) from *Torsvik et al.* [2008]. The APWPs and paleomagnetic poles are shown in Colorado (South American) Plate coordinates [*Torsvik et al.*, 2008]. The ages of the APWP mean poles are listed (in Ma). $A_{95} > 10°$ from the APWP of Gondwana have been removed for clarity. The blue circle is the Upper Choiyoi Group paleomagnetic pole (AMS tilt-corrected and anisotropy corrected). The yellow (red) circle is the anisotropy corrected Puesto Viejo Group volcanic rock paleomagnetic pole after AMS (raw) tilt-correction. The red diamond shows the Puesto Viejo Group volcaniclastic rock paleomagnetic pole after AMS tilt-correction. The orange (yellow) diamond shows the same volcaniclastic rock pole after applying an anisotropy correction of $f = 0.8$ ($f = 0.71$). Select A_{95} are shown. (b) Same as in Figure 13a, but comparing the new paleomagnetic poles against the "global" APWP of *Torsvik et al.* [2008], in Colorado Plate coordinates. (c) Comparison of the new paleomagnetic poles with an inclination-corrected ($f = 0.54$) APWP for Laurentia [*Domeier et al.*, 2011a], rotated into Colorado Plate coordinates according to *Torsvik et al.* [2008].

from the recent compilation of *Torsvik et al.* [2008], the mean 250 Ma paleopoles from Laurussia and Gondwana are separated by 20° (Figure 13a). Our new Late Permian and Early to Middle Triassic volcanic rock-based paleopoles fall between these APWPs, close to the "global" APWP that is generated by merging the Laurussian and Gondwanan data sets (Figure 13b). Specifically, the A_{95} of the Upper Choiyoi Group paleopole does not overlap with the APWP of Gondwana, but does overlap with the 265 Ma mean pole of the global APWP. The A_{95} of the Puesto Viejo Group volcanic rock-based paleopole is larger and overlaps the 245 Ma mean poles of both the Gondwanan and global APWPs, but the paleopole is closer to the latter. The position of these new volcanic-based paleopoles implies that the incongruity between the independent Laurussian and Gondwanan APWPs is due, at least in part, to bias in the paleomagnetic data from

Gondwana. Such a bias could be due to inclination shallowing in sedimentary rocks, erroneous age assignments, unrecognized remagnetizations, and/or incompletely removed viscous overprints.

[50] Inclination shallowing is especially notable because its effects are equatorially antisymmetric. Because Pangea straddles the equator in the late Paleozoic-early Mesozoic, a shallow inclination bias will drive the apparent paleolatitudes of both Laurussia and Gondwana toward the equator, resulting in an artificial separation of the APWPs when the continents are correctly restored. The paleomagnetic results from the Puesto Viejo Group volcaniclastic rocks offer an example of such effects. If the volcaniclastic rock ChRMs are not corrected for inclination shallowing, the resulting paleopole has a very high latitude, far from the global APWP (Figure 13). The A_{95} of this paleopole overlaps the 245 Ma

mean pole of the Gondwanan APWP. With the application of increasing inclination corrections (decreasing f), the latitude of the paleopole decreases and it moves toward the global APWP. Using the minimum (ATRM-determined) f-correction ($f = 0.8$), the paleopole remains close to the APWP of Gondwana, but using $f = 0.71$, the paleopole is in better accord with the global APWP. From this example, it is clear how systemic inclination shallowing, if unrecognized or under-corrected, could artificially shift the entire APWP of Gondwana away from the APWP of Laurussia. Such a systemic bias is plausible because the effects of inclination shallowing can be impossible to recognize in the absence of anisotropy measurements, robust directional analysis, or complementary igneous-based paleomagnetic results.

[51] Although a thorough analysis of Pangea reconstructions is beyond the limitations of the present study, the proximity of our new Late Permian and Early to Middle Triassic paleopoles to the global APWP of *Torsvik et al.* [2008] implies that an A-type Pangea configuration may be viable for this time. This finding concurs with several other recent studies from both Gondwana [*Brandt et al.*, 2009; *Domeier et al.*, 2011b] and Laurussia [*Meijers et al.*, 2010; *Dominguez et al.*, 2011; *Yuan et al.*, 2011; *Domeier et al.*, 2011a], which collectively show the APWPs of Gondwana and Laurussia (in an A-type reconstruction) to be converging through the progressive introduction of new, high-fidelity paleomagnetic data, and the retroactive correction of older results (Figure 13c). The obvious implication common to these studies is that alternative Pangea reconstructions and/or non-dipole paleomagnetic fields do not need to be invoked in order to accommodate the late Paleozoic-early Mesozoic paleomagnetic data from Laurussia and Gondwana, because the APWP discrepancy may simply be a manifestation of systemic bias in previous paleomagnetic results.

10. Conclusions

[52] SHRIMP U-Pb and ^{40}Ar-^{39}Ar radiogenic isotope dating has confirmed earlier age assignments of Late Permian (~264 Ma) for the Upper Choiyoi Group and Early to Middle Triassic (~245 Ma) for the Puesto Viejo Group Zircons from the Puesto Viejo Group volcanic rocks are associated with lithic fragments and are interpreted to be assimilates derived from Permian rocks during ascent and eruption of Puesto Viejo magma; their mid-to-Late Permian SHRIMP U-Pb dates do not reflect the age of Puesto Viejo Group volcanism.

[53] Field stability tests demonstrate that the ChRMs of the Upper Choiyoi Group and Puesto Viejo Group volcanic rocks are essentially primary. Field stability tests applied to the Puesto Viejo Group volcaniclastic rocks were inconclusive, but the ChRM is interpreted to be a primary DRM. Magnetic fabrics were used to discriminate between primary and secondary bedding attitudes, which ultimately improved the co-axiality of the tilt-corrected Upper Choiyoi Group and Puesto Viejo Group ChRMs. Magnetic anisotropy measurements were further utilized to correct for bias in the magnetization directions due to magnetic refraction (in the volcanic rocks) and inclination shallowing (in the volcaniclastic rocks). Rock magnetic experiments have been used to characterize the magnetic carriers, which are identified as (titano-) magnetite and hematite.

[54] The paleomagnetic poles derived from the Upper Choiyoi Group and Puesto Viejo Group volcanic rocks fall between the APWPs of Laurussia and Gondwana, near the global APWP of *Torsvik et al.* [2008]. This implies that the Late Permian-Middle Triassic APWP of Gondwana is biased by low-fidelity data and that its long-recognized separation from the APWP of Laurussia may be an artifact of such data. The paleomagnetic data derived from the Puesto Viejo Group volcaniclastic rocks serve as an illustration of this argument, in exhibiting relatively shallow inclinations that we interpret to be a consequence of sedimentary flattening of a primary DRM. A correction for the inferred shallow inclination bias results in a shift of the associated paleopole toward the global APWP of *Torsvik et al.* [2008]. These new paleomagnetic results indicate that an A-type Pangea reconstruction may be viable during the Late Permian-Middle Triassic, and that alternative paleogeographic reconstructions and/or non-dipole paleomagnetic fields are not necessary to accommodate global paleomagnetic data at this time.

References

Artabe, A. E., E. M. Morel, and D. G. Ganuza (2007), Las floras triásicas de la Argentina, *Ameghiniana*, *11*, 75–86.

Baer, E. M., R. V. Fisher, M. Fuller, and G. Valentine (1997), Turbulent transport and deposition of the Ito pyroclastic flow: Determinations using anisotropy of magnetic susceptibility, *J. Geophys. Res.*, *102*(B10), 22,565–22,586, doi:10.1029/96JB01277.

Bilardello, D., and K. P. Kodama (2010), Rock magnetic evidence for inclination shallowing in the Early Carboniferous Deer Lake Group red beds of western Newfoundland, *Geophys. J. Int.*, *181*, 275–289, doi:10.1111/j.1365-246X.2010.04537.x.

Bonaparte, J. F. (1982), Faunal replacement in the Triassic of South America, *J. Vertebr. Paleontol.*, *2*(3), 362–371, doi:10.1080/02724634.1982.10011938.

Bowles, J., M. Jackson, A. Chen, and P. Solheid (2009), Interpretation of low-temperature data part 1: Superparamagnetism and paramagnetism, *IRM Q.*, *19*(3), 1–11.

Brandt, D., M. Ernesto, A. C. Rocha-Campos, and P. R. dos Santos (2009), Paleomagnetism of the Santa Fé Group, central Brazil: Implications for the late Paleozoic apparent polar Wander path for South America, *J. Geophys. Res.*, *114*, B02101, doi:10.1029/2008JB005735.

Briden, J. C., A. G. Smith, and J. T. Sallomy (1971), The geomagnetic field in Permo-Triassic time, *Geophys. J. R. Astron. Soc.*, *23*, 101–117, doi:10.1111/j.1365-246X.1971.tb01805.x.

Cagnoli, B., and D. H. Tarling (1997), The reliability of anisotropy of magnetic susceptibility (AMS) data as flow direction indicators in friable base surge and ignimbrite deposits: Italian examples, *J. Volcanol. Geotherm. Res.*, *75*(3–4), 309–320, doi:10.1016/S0377-0273(96)00038-8.

Carvallo, C., A. R. Muxworthy, and D. J. Dunlop (2006), First order reversal curve (FORC) diagrams of magnetic mixtures: Micromagnetic models and measurements, *Phys. Earth Planet. Inter.*, *154*, 308–322, doi:10.1016/j.pepi.2005.06.017.

Cogné, J. P. (1987), TRM deviations in anisotropic assemblages of multidomain magnetite, *Geophys. J. R. Astron. Soc.*, *91*, 1013–1023.

Constable, C., and L. Tauxe (1990), The bootstrap for magnetic susceptibility tensors, *J. Geophys. Res.*, *95*(B6), 8383–8395, doi:10.1029/JB095iB06p08383.

Cortés, J. M., and L. E. Kleiman (1999), La orogenia Sanrafaélica en los Andes de Mendoza, paper presented at XIV Congreso Geológico Argentino, Univ. Nac. de Salta, Salta, Argentina.

Creer, K. M., B. J. J. Embleton, and D. A. Valencio (1970), Triassic and Permo-Triassic palaeomagnetic data for South America, *Earth Planet. Sci. Lett.*, 8, 173–178, doi:10.1016/0012-821X(70)90169-X.

Creer, K. M., J. G. Mitchell, and D. A. Valencio (1971), Evidence for a normal geomagnetic field polarity event at 263 ± 5 m.y. B.P. within the late Paleozoic reversed interval, *Nature*, 233, 87–89.

De Fauw, S. L. (1993), The Pangean dicynodont *Rechnisaurus* from the Triassic of Argentina, in *The Nonmarine Triassic*, edited by S. G. Lucas and M. Morales, *N. M. Mus. of Nat. Hist. and Sci. Bull.*, 3, 101–105.

Domeier, M., R. Van der Voo, and B. Denny (2011a), Widespread inclination shallowing in Permian and Triassic paleomagnetic data from Laurentia? Support from a shallow intrusive record and virtual geomagnetic pole distributions, *Tectonophysics*, 511, 38–52, doi:10.1016/j.tecto.2011.08.016.

Domeier, M., R. Van der Voo, E. Tohver, R. Tomezzoli, H. Vizan, T. Torsvik, and J. Kirshner (2011b), New Late Permian paleomagnetic data from Argentina refine the apparent polar wander path of Gondwana, *Geochem. Geophys. Geosyst.*, 12, Q07002, doi:10.1029/2011GC003616.

Dominguez, A. R., R. Van der Voo, T. H. Torsvik, B. W. H. Hendriks, A. Abrajevitch, M. Domeier, B. T. Larsen, and S. Rousse (2011), The ∼270 Ma palaeolatitude of Baltica and its significance for Pangea models, *Geophys. J. Int.*, 186, 529–550, doi:10.1111/j.1365-246X.2011.05061.x.

Domnanovich, N., and C. Marsicano (2009), Los dicinodontes (Amniota: Terápsia) de Argentina: Síntesis sobre el conocimiento actual del grupo, *Ameghiniana*, 40, 55.

Dormann, J., D. Fiorani, and E. Tronc (1997), Magnetic relaxation in fine particle systems, in *Advances in Chemical Physics (98)*, edited by I. Prigogine and S. Rice, pp. 283–494, John Wiley, Hoboken, N. J., doi:10.1002/9780470141571.ch4.

Ellwood, B. B. (1982), Estimates of flow direction for calc-alkaline welded tuffs and paleomagnetic data reliability from anisotropy of magnetic susceptibility measurements: Central San Juan Mountains, southwest Colorado, *Earth Planet. Sci. Lett.*, 59, 303–314, doi:10.1016/0012-821X(82)90133-9.

Ericsson, T., A. Krisnhamurthy, and B. K. Srivastava (1986), Morin-transition in Ti-substituted hematite: A Mössbauer study, *Phys. Scr.*, 33(1), 88, doi:10.1088/0031-8949/33/1/013.

Ezcurra, M. D., A. Lecuona, and A. G. Martinelli (2010), A new basal archosauriform diapsid from the lower Triassic of Argentina, *J. Vertebr. Paleontol.*, 30(5), 1433–1450, doi:10.1080/02724634.2010.501446.

Fisher, R. A. (1953), Dispersion on a sphere, *Proc. R. Soc. London A*, 217, 295–305, doi:10.1098/rspa.1953.0064.

González Díaz, E. P. (1972), Descripción geológica de la Hoja 27d, San Rafael. Provincia de Mendoza, *Bol. Serv. Min. Nac.*, 132, 1–127.

Gradstein, F. M., J. G. Ogg, and A. G. Smith (2004), *A Geologic Time Scale 2004*, 610 pp., Cambridge Univ. Press, Cambridge, U. K.

Grégoire, V., J. Darrozes, P. Gaillot, A. Nédélec, and P. Launeau (1998), Magnetite grain shape fabric and distribution anisotropy vs rock magnetic fabric: A three-dimensional case study, *J. Struct. Geol.*, 20(7), 937–944, doi:10.1016/S0191-8141(98)00022-4.

Hrouda, F. (1982), Magnetic anisotropy of rocks and its application in geology and geophysics, *Geophys. Surv.*, 5(1), 37–82, doi:10.1007/BF01450244.

Incoronato, A., F. T. Addison, D. H. Tarling, G. Nardi, and T. Pescatore (1983), Magnetic fabric investigations of pyroclastic deposits from phlegrean fields, southern Italy, *Nature*, 306, 461–463, doi:10.1038/306461a0.

Irving, E. (1977), Drift of the major continental blocks since the Devonian, *Nature*, 270, 304–309, doi:10.1038/270304a0.

Irving, E. (2004), The case for Pangea B, and the intra-Pangean megashear, in *Timescales of the Paleomagnetic Field*, *Geophys. Monogr. Ser.*, vol. 145, edited by J. E. T. Channell et al., pp. 13–27, AGU, Washington, D. C., doi:10.1029/145GM02.

Jackson, M. (1991), Anisotropy of magnetic remanence: A brief review of mineralogical sources, physical origins, and geological applications, and comparison with susceptibility anisotropy, *Pure Appl. Geophys.*, 136(1), 1–28, doi:10.1007/BF00878885.

Jacob, J., and M. Abdul Khadar (2010), VSM and mössbauer study of nanostructured hematite, *J. Magn. Magn. Mater.*, 322(6), 614–621, doi:10.1016/j.jmmm.2009.10.025.

Japas, M. S., J. Salvarredi, and L. E. Kleiman (2005), Self-similar behaviour of Triassic rifting in San Rafael, Mendoza, Argentina, paper presented at Gondwana XII, Acad. Nac. de Cienc., Mendoza, Argentina.

Jelinek, K. (1981), Characterization of the magnetic fabric of rocks, *Tectonophysics*, 79, T63–T67, doi:10.1016/0040-1951(81)90110-4.

Khan, M. A. (1962), The anisotropy of magnetic susceptibility of some igneous and metamorphic rocks, *J. Geophys. Res.*, 67(7), 2873–2885, doi:10.1029/JZ067i007p02873.

King, R. (1955), The remanent magnetism of artificially deposited sediments, *Geophys. J. Int.*, 7, 115–134, doi:10.1111/j.1365-246X.1955.tb06558.x.

Kleiman, L. E. (2002), Magmatism and tectonic evolution of the Choiyoi and Puesto Viejo volcanics (Late Paleozoic-Early Mesozoic) at 34–35°S latitude, San Rafael, Mendoza, Argentina, paper presented at XV Congreso Geológico Argentino, El Calafate, Argentina.

Kleiman, L. E., and M. S. Japas (2005), The upper Choyoi volcanism, San Rafael, Mendoza, Argentina: A transitional sequence emplaced under changing geodynamic conditions, paper presented at Gondwana XII, Acad. Nac. de Cienc., Mendoza, Argentina.

Kleiman, L. E., and M. S. Japas (2009), The Choiyoi volcanic province at 34°S–36°S (San Rafael, Mendoza, Argentina): Implications for the late Palaeozoic evolution of the southwestern margin of Gondwana, *Tectonophysics*, 473, 283–299, doi:10.1016/j.tecto.2009.02.046.

Kleiman, L. E., and J. A. Salvarredi (1999), Triassic bimodal volcanism in the San Rafael Massif, Mendoza: The Puesto Viejo Formation, paper presented at XIV Congreso Geológico Argentino, Univ. Nac. de Salta, Salta, Argentina.

Kleiman, L. E., and J. A. Salvarredi (2001), Petrology, geochemistry and tectonic implications of Triassic volcanism (Puesto Viejo Formation), San Rafael Massif, Mendoza, *Asoc. Geol. Argent. Rev.*, 56(4), 559–570.

Le Pennec, J., Y. Chen, H. Diot, J. Froger, and A. Gourgaud (1998), Interpretation of anisotropy of magnetic susceptibility fabric of ignimbrites in terms of kinematic and sedimentological mechanisms: An Anatolian case-study, *Earth Planet. Sci. Lett.*, 157, 105–127, doi:10.1016/S0012-821X(97)00215-X.

Linares, E. (2007), Catálogo de edades radimétricas de la República Argentina, *Años 1957–2005*, Asoc. Geol. Argent., Buenos Aires.

Lucas, S. G. (1998), Global Triassic tetrapod biostratigraphy and biochronology, *Palaeogeogr. Palaeoclimatol. Palaeoecol.*, 143, 347–384, doi:10.1016/S0031-0182(98)00117-5.

Martinelli, A. G. (2010), On the postcanine dentition of *Pascualgnathus polanskii* Bonaparte (Cynodontia, Traversodontidae) from the Middle Triassic of Argentina, *Geobios*, 43, 629–638, doi:10.1016/j.geobios.2010.03.006.

Martinelli, A. G., M. de la Fuente, and F. Abdala (2009), *Diademodon tetragonus* Seeley, 1894(Therapsida: Cynodontia) in the Triassic of South America and its biostratigraphic implications, *J. Vertebr. Paleontol.*, 29(3), 852–862, doi:10.1671/039.029.0315.

Meijers, M. J. M., M. F. Hamers, D. J. J. van Hinsbergen, D. G. van der Meer, A. Kitchka, C. G. Langereis, and R. A. Stephenson (2010), New late Paleozoic paleopoles from the Donbas Foldbelt (Ukraine): Implications for the Pangea A vs. B controversy, *Earth Planet. Sci. Lett.*, 297, 18–33, doi:10.1016/j.epsl.2010.05.028.

Melchor, R. N. (2000), Stratigraphic and biostratigraphic consequences of a new ^{40}Ar/^{39}Ar date for the base of the Cochico Group (Permian), eastern Permian basin, San Rafael, Mendoza, Argentina, *Ameghiniana*, 37, 271–282.

Morel, P., and E. Irving (1981), Paleomagnetism and the evolution of Pangea, *J. Geophys. Res.*, 86(B3), 1858–1872, doi:10.1029/JB086iB03p01858.

Moskowitz, B. M., M. Jackson, and C. Kissel (1998), Low-temperature magnetic behavior of titanomagnetites, *Earth Planet. Sci. Lett.*, 157, 141–149, doi:10.1016/S0012-821X(98)00033-8.

Muttoni, G., D. V. Kent, E. Garzanti, P. Brack, N. Abrahamsen, and M. Gaetani (2003), Early Permian Pangea "B" to late Permian Pangea "A", *Earth Planet. Sci. Lett.*, 215, 379–394, doi:10.1016/S0012-821X(03)00452-7.

Muttoni, G., et al. (2009), Opening of the neo-tethys ocean and the Pangea B to Pangea A transformation during the Permian, *GeoArabia*, 14(4), 17–48.

Muxworthy, A. R., and E. McClelland (2000), Review of the low-temperature magnetic properties of magnetite from a rock magnetic perspective, *Geophys. J. Int.*, 140, 101–114, doi:10.1046/j.1365-246x.2000.00999.x.

Opdyke, N. D., J. Roberts, J. Claoue-Long, E. Irving, and P. J. Jones (2000), Base of the Kiaman: Its definition and global stratigraphic significance, *Geol. Soc. Am. Bull.*, 112, 1315–1341, doi:10.1130/0016-7606(2000)112<1315:BOTKID>2.0.CO;2.

Ort, M. H., G. Orsi, L. Pappalardo, and R. V. Fisher (2003), Anisotropy of magnetic susceptibility studies of depositional processes in the Campanian Ignimbrite, Italy, *Bull. Volcanol.*, 65(1), 55–72.

Ottone, E. G., and G. B. Garcia (1991), A lower Triassic miospore assemblage from the Puesto Viejo Formation, Argentina, *Rev. Palaeobot. Palynol.*, 68, 217–232, doi:10.1016/0034-6667(91)90025-X.

Özdemir, Ö., D. J. Dunlop, and T. S. Berquó (2008), Morin transition in hematite: Size dependence and thermal hysteresis, *Geochem. Geophys. Geosyst.*, 9, Q10Z01, doi:10.1029/2008GC002110.

Palmer, H. C., and W. D. MacDonald (1999), Anisotropy of magnetic susceptibility in relation to source vents of ignimbrites: Empirical observations, *Tectonophysics*, 307, 207–218, doi:10.1016/S0040-1951(99)00126-2.

Pioli, L., R. Lanza, M. Ort, and M. Rosi (2008), Magnetic fabric, welding texture and strain fabric in the Nuraxi Tuff, Tardinia, Italy, *Bull. Volcanol.*, 70(9), 1123–1137, doi:10.1007/s00445-008-0194-1.

Renne, P. R., R. Mundil, G. Balco, K. Min, and K. R. Ludwig (2010), Joint determination of ^{40}K decay constants and ^{40}Ar*/^{40}K for the Fish Canyon sanidine standard, and improved accuracy for ^{40}Ar/^{39}Ar geochronology, *Geochim. Cosmochim. Acta*, *74*(18), 5349–5367, doi:10.1016/j.gca.2010. 06.017.

Roberts, A. P., C. R. Pike, and K. L. Verosub (2000), First-order reversal curve diagrams: A new tool for characterizing the magnetic properties of natural samples, *J. Geophys. Res.*, *105*(B12), 28,461–28,475, doi:10.1029/ 2000JB900326.

Rocha-Campos, A. C., et al. (2011), 30 million years of Permian volcanism recorded in the Choiyoi igneous province (W. Argentina) and their source for younger ash fall deposits in the Paraná Basin: SHRIMP U–Pb zircon geochronology evidence, *Gondwana Res.*, *19*(2), 509–523, doi:10.1016/j. gr.2010.07.003.

Rochette, P., and D. Vandamme (2001), Pangea B: An artifact of incorrect paleomagnetic assumptions?, *Ann. Geofis.*, *44*(3), 649–658.

Rochette, P., M. Jackson, and C. Aubourg (1992), Rock magnetism and the interpretation of anisotropy of magnetic susceptibility, *Rev. Geophys.*, *30*(3), 209–226, doi:10.1029/92RG00733.

Sepúlveda, E., F. Carpio, M. Regairaz, M. Zárate, and J. C. Zanettini (2007), Hoja Geológica 3569 - II, San Rafael, Provincia de Mendoza, *Bull. 321*, 59 p., Inst. de Geol. y Recursos Miner., Serv. Geol. Min. Argent., Buenos Aires.

Smith, A. G., and R. A. Livermore (1991), Pangea in Permian to Jurassic time, *Tectonophysics*, *187*, 135–179, doi:10.1016/0040-1951(91)90417-Q.

Spalletti, L. A., J. C. Merodio, S. D. Matheos, and A. M. Iñiguez Rodriguez (1996), Petrology and geochemistry of Triassic silicoclastic sediments from the Sierra Pintada, Mendoza Province, *Asoc. Geol. Argent. Rev.*, *51*(1), 51–60.

Stipanicic, P. N., E. F. González Díaz, and A. M. Zavattieri (2007), Grupo Puesto Viejo nom. transl por Formación Puesto Viejo González Díaz, 1964–1967: Nuevas interpretaciones paleontológicas, estratigráficas y cronológicas, *Ameghiniana*, *44*, 759–761.

Tarling, D. H., and F. Hrouda (1993), *The Magnetic Anisotropy of Rocks*, Chapman and Hall, London.

Tauxe, L., and G. S. Watson (1994), The fold test: An eigen analysis approach, *Earth Planet. Sci. Lett.*, *122*, 331–341, doi:10.1016/0012- 821X(94)90006-X.

Tauxe, L., T. A. T. Mullender, and T. Pick (1996), Potbellies, wasp-waists, and superparamagnetism in magnetic hysteresis, *J. Geophys. Res.*, *101*(B1), 571–583, doi:10.1029/95JB03041.

Tauxe, L., K. P. Kodama, and D. V. Kent (2008), Testing corrections for paleomagnetic inclination error in sedimentary rocks: A comparative approach, *Phys. Earth Planet. Inter.*, *169*, 152–165, doi:10.1016/j.pepi. 2008.05.006.

Terrizzano, C. M., R. N. Tomezzoli, L. Kleiman, and J. Salvarredi (2005), Resultados paleomagnéticos preliminares sobre rocas de la Quebrada del Pimiento, Bloque de San Rafael, Provincia de Mendoza, Argentina, paper presented at XVI Congreso Geológico Argentino, Asoc. Geol. Argentina, Buenos Aires.

Tomezzoli, R. N., L. Kleiman, J. Salvarredi, C. Terrizzano, and O. Cristallini (2005), Relaciones estratigráicas de volcanitas del Choiyoi Inferior sobre la base de estudios paleomagnéticos, Bloque de San Rafael, Mendoza, Argentina, paper presented at XVI Congreso Geológico Argentino, Asoc. Geol. Argentina, Buenos Aires.

Torcq, F., et al. (1997), Paleomagnetic results from Saudi Arabia and the Permo-Triassic Pangea configuration, *Earth Planet. Sci. Lett.*, *148*, 553–567, doi:10.1016/S0012-821X(97)00047-2.

Torsvik, T. H., and R. Van der Voo (2002), Refining Gondwana and Pangea palaeogeography: Estimates of Phanerozoic non-dipole (octupole) fields, *Geophys. J. Int.*, *151*, 771–794, doi:10.1046/j.1365-246X.2002. 01799.x.

Torsvik, T. H., R. D. Muller, R. Van der Voo, B. Steinberger, and C. Gaina (2008), Global plate motion frames: Toward a unified model, *Rev. Geophys.*, *46*, RG3004, doi:10.1029/2007RG000227.

Valencio, D. A., and J. Mitchell (1972), Edad potasio-argon y paleomagnetismo de rocas igneas de las Formaciones Quebrada del Pimiento y Las Cabras, provincia de Mendoza, Republica Argentina, *Asoc. Geol. Argent. Rev.*,*27*(2), 170–178.

Valencio, D. A., J. E. Mendia, and J. F. Vilas (1975), Palaeomagnetism and K-Ar ages of Triassic igneous rocks from the Ischigualasto-Ischichuca Basin and Puesto Viejo Formation, Argentina, *Earth Planet. Sci. Lett.*, *26*, 319–330, doi:10.1016/0012-821X(75)90007-2.

Van der Voo, R., and T. H. Torsvik (2001), Evidence for late Paleozoic and Mesozoic non-dipole fields provides an explanation for the Pangea reconstruction problems, *Earth Planet. Sci. Lett.*, *187*, 71–81, doi:10.1016/ S0012-821X(01)00285-0.

Van der Voo, R., and T. H. Torsvik (2004), The quality of the European Permo-Triassic paleopoles and its impact on Pangea reconstructions. Timescales of the paleomagnetic field, in *Timescales of the Paleomagnetic Field*, *Geophys. Monogr. Ser.*, vol. 145, edited by J. E. T. Channell et al., pp. 29–42, AGU, Washington, D. C., doi:10.1029/145GM03.

Vilas, J. F., and D. A. Valencio (1982), Implicancias geodinámicas de los resultados paleomagneticos de formaciones asignadas al Paleozoico tardío-Mesozoico temprano del Centro-Oeste Argentino, paper presented at V Congreso Latinoamericano de Geología, Asoc. Geol. Argent., Buenos Aires.

Watson, B. E. (1996), Dissolution, growth and survival of zircons during crustal fusion: Kinetic principles, geological models and implications for isotopic inheritance, *Spec. Pap. Geol. Soc. Am.*, *315*, 43–56.

Watson, G. S. (1956), A test for randomness of directions. Monthly Notices of the Royal Astronomical Society, *Geophys. J. Int.*, *7*,160–161, doi:10.1111/j.1365-246X.1956.tb05561.x.

Yuan, K., R. Van der Voo, M. L. Bazhenov, V. Bakhmutov, V. Alekhin, and B. W. H. Hendriks (2011), Permian and Triassic palaeolatitudes of the Ukrainian shield with implications for Pangea reconstructions, *Geophys. J. Int.*, *184*, 595–610, doi:10.1111/j.1365-246X.2010.04889.x.

Zavattieri, A. M., and D. J. Batten (1996), Miospores from Argentinian Triassic deposits and their potential for intercontinental correlation, in *Palynology: Principles and Applications*, vol. 2, edited by J. Jansonius and D. C. McGregor, pp. 767–778, Am. Assoc. of Stratigr. Palynol. Found., College Station, Tex.

M. Domeier, A. Dominguez, and R. Van der Voo, Department of Earth and Environmental Sciences, University of Michigan, Ann Arbor, MI 48109-1005, USA. (domeier@umich.edu; voo@umich.edu; ardomin@umich.edu)

B. W. H. Hendriks, Geological Survey of Norway, PO Box 6315 Sluppen, N-7491 Trondheim, Norway. (bart.hendriks@ngu.no)

E. Tohver, School of Earth and Geographical Sciences, University of Western Australia, 35 Stirling Hwy., Crawley, WA 6009, Australia. (etohver@cyllene.uwa.edu.au)

R. N. Tomezzoli and H. Vizan, Departamento de Ciencias Geológicas, Universidad de Buenos Aires, Pabellón 2, Ciudad Universitaria, Buenos Aires C.P. 1428, Argentina. (renata@gl.fcen.uba.ar; haroldo@gl.fcen.uba.ar)

T. H. Torsvik, Department of Physics, University of Oslo, PO Box 1047 Blindern, N-0316, Oslo, Norway. (t.h.torsvik@geo.uio.no)